E4F1 deficiency results in oxidative stress–mediated cell death of leukemic cells

Elodie Hatchi,[1] Genevieve Rodier,[1] Matthieu Lacroix,[2] Julie Caramel,[1] Olivier Kirsh,[1] Chantal Jacquet,[1] Emilie Schrepfer,[2] Sylviane Lagarrigue,[1] Laetitia Karine Linares,[2] Gwendaline Lledo,[2] Sylvie Tondeur,[4] Pierre Dubus,[3] Claude Sardet,[1] and Laurent Le Cam[1,2]

[1]Institut de Génétique Moléculaire de Montpellier, Centre National de la Recherche Scientifique Unité Mixte de Recherche 5535, Institut Fédératif de Recherche 122, Université de Montpellier, Montpellier 34293, France
[2]Institut de Recherche en Cancérologie de Montpellier, Institut National de la Santé et de la Recherche Médicale Unité 896, Centre Régional de Lutte contre le Cancer Val d'Aurelle–Paul Lamarque, Université Montpellier 1, Montpellier 34298, France
[3]Université Victor Segalen, Bordeaux 33076, France
[4]Laboratoire d'Hématologie, Hôpital St. Eloi, Centre Hospitalier Universitaire, Montpellier 34295, France

The multifunctional E4F1 protein was originally discovered as a target of the E1A viral oncoprotein. Growing evidence indicates that E4F1 is involved in key signaling pathways commonly deregulated during cell transformation. In this study, we investigate the influence of E4F1 on tumorigenesis. Wild-type mice injected with fetal liver cells from mice lacking *CDKN2A*, the gene encoding Ink4a/Arf, developed histiocytic sarcomas (HSs), a tumor originating from the monocytic/macrophagic lineage. Cre-mediated deletion of *E4F1* resulted in the death of HS cells and tumor regression in vivo and extended the lifespan of recipient animals. In murine and human HS cell lines, *E4F1* inactivation resulted in mitochondrial defects and increased production of reactive oxygen species (ROS) that triggered massive cell death. Notably, these defects of E4F1 depletion were observed in HS cells but not healthy primary macrophages. Short hairpin RNA–mediated depletion of E4F1 induced mitochondrial defects and ROS-mediated death in several human myeloid leukemia cell lines. E4F1 protein is overexpressed in a large subset of human acute myeloid leukemia samples. Together, these data reveal a role for *E4F1* in the survival of myeloid leukemic cells and support the notion that targeting E4F1 activities might have therapeutic interest.

CORRESPONDENCE
Laurent Le Cam:
laurent.lecam@inserm.fr
OR
Claude Sardet:
claude.sardet@igmm.cnrs.fr

Abbreviations used: 3MA, 3-methyladenine; 4OHT, 4-hydroxy-tamoxifen; 8-OHdG, 8-hydroxy-2′-deoxyguanosine; AML, acute myeloid leukemia; AO, acridine orange; D3T, 3H-1,2 dithiole-3-thione; DCFDA, 2′,7′-dichlorofluorescein diacetate; HS, histiocytic sarcoma; HSC, hematopoietic stem cell; IHC, immunohistochemistry; KI, knockin; mRNA, messenger RNA; NAC, *N*-acetyl-L-cysteine; OCR, oxygen consumption rate; PET, positron emission tomography; PI, propidium iodide; PI3K, phosphoinositide 3-kinase; qPCR, quantitative PCR; ROS, reactive oxygen species; shRNA, short hairpin RNA; TUNEL, terminal deoxynucleotidyl transferase biotin-dUTP nick end labeling.

Pioneer work on viral oncoproteins led to the discovery in the 1980s of several essential regulators of cell division and cell survival. Among those, E4F1 was originally identified as a cellular target of the E1A viral oncoprotein during adenoviral infection and was originally characterized for its implication in the transcriptional regulation of the viral E4 promoter (Lee and Green, 1987; Lee et al., 1987; Raychaudhuri et al., 1987). In addition to its intrinsic transcriptional activities (Fajas et al., 2001; Ahmed-Choudhury et al., 2005), E4F1 also exhibits an atypical ubiquitin E3 ligase function that targets other transcription factors, including the p53 tumor suppressor (Le Cam et al., 2006). Although the complex transcriptional program regulated by E4F1 remains poorly understood, E4F1 is implicated in several steps controlling cell cycle progression in both somatic and embryonic cells (Fernandes et al., 1998; Rooney, 2001; Le Cam et al., 2004). Furthermore, *E4F1* was recently shown to be essential for epidermal stem cell maintenance and proper skin homeostasis in murine epidermis (Lacroix et al., 2010).

Growing evidences suggest that E4F1 is implicated in carcinogenesis. Consistent with that notion, E4F1 was found to be regulated by and/or to interact with several viral oncoproteins, including E1A13S (adenovirus serotype V; Raychaudhuri et al., 1987), GAM1 (adenovirus Celo; Colombo et al., 2003), and HBX (hepatitis virus B; Rui et al., 2006). In addition, E4F1 is involved in several essential oncogenic pathways, including the RB and p53 tumor suppressor pathways. Indeed, inactivation of *Rb*

The Rockefeller University Press $30.00
J. Exp. Med. Vol. 208 No. 7 1403-1417
www.jem.org/cgi/doi/10.1084/jem.20101995

The Journal of Experimental Medicine

decreases E4F1 antiproliferative activities (Fajas et al., 2000), and E4F1 impinges on the p53 pathway at different levels. Thus, through its atypical ubiquitin E3 ligase domain, E4F1 modulates p53 transcriptional activities independently of degradation and modulates its effector functions involved in alternative cell fates: growth arrest or apoptosis (Sandy et al., 2000; Le Cam et al., 2006). E4F1 also directly interacts with upstream regulators of the p53 pathway such as the polycomb member Bmi1 (Chagraoui et al., 2006), a transcriptional repressor of the *CDKN2A* locus (also referred to as the *Ink4a/Arf* locus), as well as with one of its encoded proteins, the $p14^{ARF}$ tumor suppressor (Rizos et al., 2003). Finally, E4F1 interacts with the p53 target gene product FHL2/Dral that modulates E4F1-p53 binding (Paul et al., 2006).

Although they play important roles in E4F1-associated activities, genetic evidence indicates that *E4F1* functions extend beyond the Rb and p53 pathways. Thus, functional inactivation of either pathway only partly rescues phenotypes associated with E4F1 gain or loss of functions. Consistent with that notion, peri-implantation lethality of *E4F1* KO embryos is not rescued by concomitant inactivation of *p53* (unpublished data), and *E4F1* KO epidermal stem cell defects are partly but not fully rescued upon genetic inactivation of the p53 pathway (Lacroix et al., 2010). Recent data also suggest that E4F1 participates in other oncogenic pathways, as shown by its direct interaction with several tumor suppressors or oncogenes, including RASSF1A (Fenton et al., 2004; Ahmed-Choudhury et al., 2005), HNF1 (Dudziak et al., 2008), SMAD4 (Nojima et al., 2010), and HMGA2 (Tessari et al., 2003). Thus, those interactions raise the question about E4F1 functions that are independent of the Rb and p53 pathways, in particular during tumor development.

In this study, we started to address the importance of *E4F1* during tumorigenesis, using a mouse model harboring a genetic alteration of the *Ink4a/Arf* locus. By virtue of specific promoters and first exons, this locus generates two transcripts with distinct open reading frames encoding the $p16^{INK4a}$ and ARF proteins that exhibit independent but synergistic tumor suppressor activities through their implication in the Rb and p53 pathways, respectively (Quelle et al., 1995; Kamijo et al., 1997; Sharpless et al., 2001; Kim and Sharpless, 2006; Berger and Bardeesy, 2007). Loss of the *Ink4a/Arf* locus or functional inactivation of its encoded proteins occurs in a wide spectrum of human tumors, including melanoma, pancreatic adenocarcinoma, glioblastoma, lung cancer, bladder carcinoma, and lymphoid and myeloid leukemias (Kim and Sharpless, 2006). In this study, we addressed the direct implication of *E4F1* in leukemic development in a tumor-prone mouse model resulting from *Ink4a/Arf* inactivation. In that model, as well as in several human myeloid leukemia cell lines, *E4F1* inactivation resulted in mitochondrial defects and oxidative stress–mediated cell death. In addition, we found that E4F1 is overexpressed in a large subset of human acute myeloid leukemias (AMLs). Altogether, our data show an important function of *E4F1* in tumor cell survival.

RESULTS

Development of a mouse histiocytic sarcoma (HS) model harboring the E4F1 conditional KO allele

To study *E4F1* functions during tumorigenesis, we used a recently developed genetically engineered mouse model containing *E4F1*-null and *E4F1* conditional KO alleles ($E4F1^{-/flox}$) based on the Cre/Lox-P technology (Fig. 1 A and Fig. S1 A; Le Cam et al., 2004; Lacroix et al., 2010). $E4F1^{-/flox}$ mice were crossed with RERT mice, a knockin (KI) strain expressing the 4-hydroxy-tamoxifen (4OHT)–inducible $Cre\text{-}ER^{T2}$ fusion protein under the control of the ubiquitously active promoter of the *RNA polymerase II* large subunit gene (Guerra et al., 2003). In vivo recombination efficiency of the $E4F1^{flox}$ allele was assessed in several organs of $E4F1^{-/flox}$; $RERT^{KI/KI}$ mice by quantitative PCR (qPCR) on genomic DNA, RT-qPCR on purified RNA, or Western blot analyses of total protein extracts (Fig. 1 B and Fig. S1 A). Upon 4OHT administration, high recombination efficiency was detected in several organs, including liver, spleen, and lungs, as well as in peripheral white blood cells and total or purified lineage-negative (Lin^-) BM cells (Fig. 1 B). These analyses validated our model and confirmed that *E4F1* is efficiently deleted upon Cre activation in the hematopoietic compartment. However, analyses of $E4F1^{-/flox}$; $RERT^{KI/KI}$ mice also revealed critical roles of *E4F1* in other organs, limiting long-term investigations of phenotypes resulting from *E4F1* loss in the hematopoietic compartment in that mouse model.

To address *E4F1* functions during tumorigenesis, we next crossed $E4F1^{flox}$; $RERT^{KI/KI}$ animals with *Ink4a/Arf* KO mice. The latter strain of mice harbors a deletion of exons 2 and 3 of the *Ink4a/Arf* locus and therefore expresses neither $p16^{INK4a}$ nor $p19^{ARF}$. *Ink4a/Arf*-null animals are tumor prone and were previously described to develop with high penetrance essentially B and T cell lymphomas and soft tissue sarcomas with an expected mean age of tumor appearance around 30 wk (Serrano et al., 1996). To avoid defects resulting from *E4F1* inactivation in the whole organism and investigate *E4F1* functions during tumorigenesis, we transplanted fetal liver hematopoietic stem cells (HSCs) isolated from $E4F1^{-/flox}$; $RERT^{KI/KI}$; $Ink4a/Arf^{-/-}$ embryos or their control $E4F1^{+/flox}$; $RERT^{KI/KI}$; $Ink4a/Arf^{-/-}$ littermates into lethally irradiated WT recipient mice (herein referred to as *E4F1* KO or CT; *Ink4a/Arf* KO mice, according to the genotype of the transplanted cells). We used this strategy to generate several cohorts of tumor-prone mice in which *E4F1* could be acutely inactivated specifically in the hematopoietic system and in tumors derived from those cells upon administration of 4OHT (Fig. S1 B).

We then carefully monitored our transplanted mice for perturbations of the hematopoietic system and for tumor susceptibility. Strikingly, we found that our cohorts of transplanted animals, regardless of *E4F1* genotype and in the absence of 4OHT administration, developed with full penetrance HSs, a tumor type originating from the monocytic/macrophagic lineage, but no B nor T cell lymphomas. These tumors arose as soon as 10 wk after transplantation, and postmortem histological analyses indicated that all transplanted

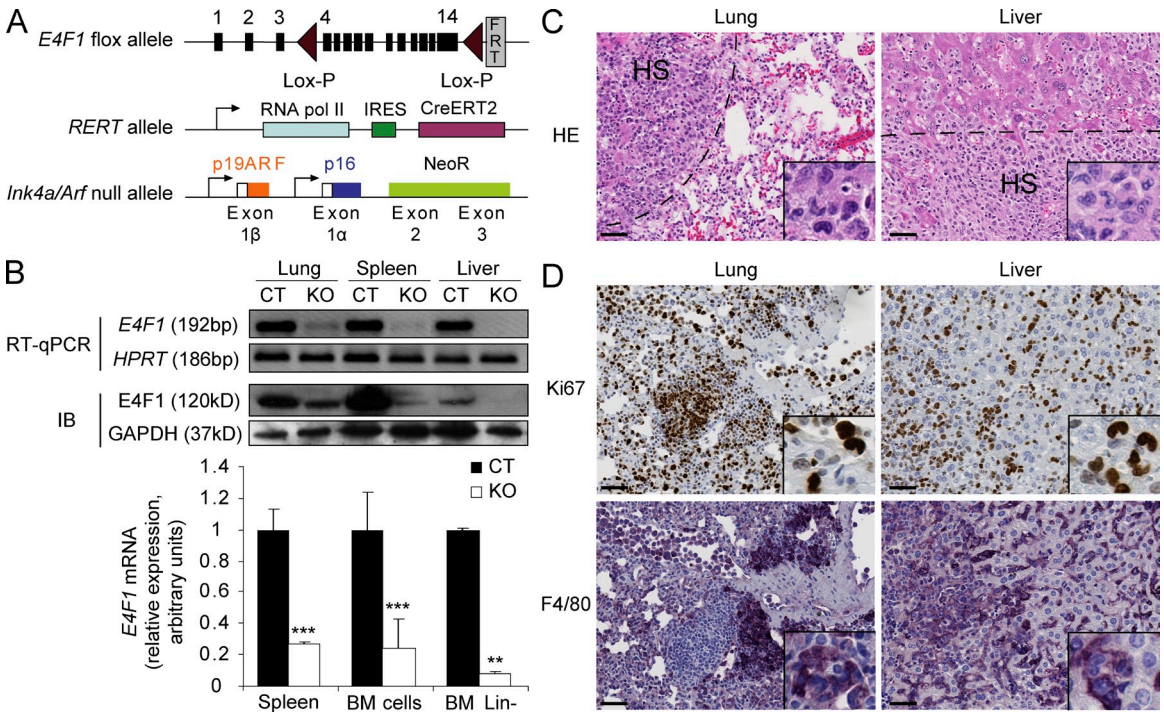

Figure 1. Development of a mouse model of HS harboring the *E4F1* conditional KO allele. (A) Schematic representation of the different *E4F1*^{flox}, *RERT* KI, and *Ink4a/Arf*-null alleles. (B) RT-qPCR and immunoblot (IB) analyses of E4F1 expression in tissues isolated from *E4F1*$^{+/flox}$; *RERT*$^{KI/KI}$ (CT) or *E4F1*$^{-/flox}$; *RERT*$^{KI/KI}$ (KO) mice after repeated administration of 4OHT. RT-qPCR products were loaded on agarose gels (top) after real-time PCR amplification to verify fragment size and purity of amplicons. *HPRT* mRNA and GAPDH protein were used to normalize RT-qPCR and immunoblots, respectively. Bar graph shows mean ± SD (n = 3) of RT-qPCR data. BM cells represent total BM cells. BM Lin$^-$ (lineage negative) cells represent a fraction of purified BM cells enriched in HSCs and progenitor cells that were negatively selected for expression of lineage-specific markers (CD3, B220, Ter119, Gr-1, and Mac1). **, P < 0.01; ***, P < 0.001. (C) Microphotographs of representative H&E-stained histological lung and liver sections from transplanted mice. Dashed lines indicate the edge of the infiltrating HS. Insets show high-magnification images of HS cells exhibiting large eosinophilic cytoplasm and reniform nucleus. (D) Immunophenotypical analysis of HS. Representative tumors observed in the lung and liver were analyzed by IHC using antibodies for the proliferation marker Ki67 (brown staining) and the histiocytic marker F4/80 (dark purple staining), as indicated. Insets show high-magnification images of HS cells. Bars, 50 µm.

animals showed diffuse and/or nodular neoplastic infiltrations in the spleen, liver, or lungs. Pathological analyses of tumors recovered from reconstituted animals confirmed that they exhibited all phenotypic and immunological features reminiscent of human HSs, according to the international World Health Organization classification of human tumors. HS tumor cells appeared as large cells with abundant eosinophilic cytoplasm and pleiomorphic nuclei with large nucleoli (Fig. 1 C) and showed positive immunoreactivity with the histiocytic cell surface markers F4/80 and/or Mac2 and heterogenous staining for the proliferation marker Ki67 (Fig. 1 D and Fig. 2 B). All tumors stained negative for B and T cell markers (Fig. S1 D), indicating that none of the transplanted animals developed the previously described B or T cell lymphoma spectrum found in *Ink4a/Arf* KO animals (Serrano et al., 1996). Increased number of F4/80-positive HS cells was also detected by flow cytometry in the peripheral blood between 10 and 20 wk after transplantation and indicated the progression of the disease (Fig. S1 F). Finally, most of these transplanted animals exhibited profound anemia and body weight loss at late stages of tumor progression (unpublished data). Death of those animals occurred between 3 and 11 mo after transplantation, according to *E4F1* status (Fig. 2 A).

Altogether, these data indicated that we established a novel murine HS model based on transplantation of *Ink4a/Arf*-null fetal liver HSCs. Tumors that developed in that animal model also harbored the *E4F1* conditional KO allele, allowing us to address the roles of *E4F1* during tumor development.

E4F1 inactivation results in decreased tumor development and increased life span

Next, we addressed the consequences of *E4F1* inactivation in transplanted animals. For evaluation of tumor susceptibility, recipient mice were transplanted with fetal HSCs harvested from genetically matched *E4F1*$^{+/flox}$ or *E4F1*$^{-/flox}$; *RERT*$^{KI/KI}$; *Ink4a/Arf*$^{+/+}$ or *Ink4a/Arf*$^{-/-}$ mice (herein referred to as *E4F1* CT or KO; *Ink4a/Arf* WT or KO, according to the genotype of the transplanted cells). In the first experimental group, 4OHT was administered in reconstituted animals 10 wk after transplantation to allow full reconstitution of the hematopoietic system before Cre-mediated recombination. Administration of 4OHT was then repeated on a monthly basis until the death of the animals (Fig. S1 B).

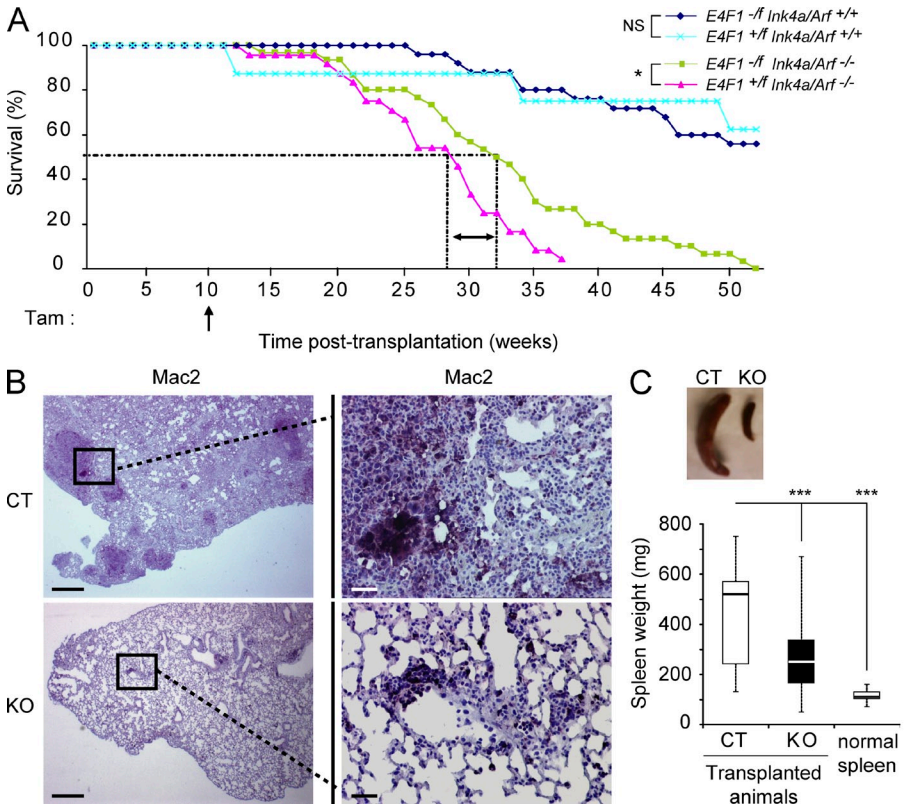

Figure 2. *E4F1* inactivation results in decreased tumor development and increased lifespan. (A) Kaplan-Meier survival curve of recipients transplanted with fetal liver cells from *E4F1*$^{+/flox}$; *Ink4a/Arf*$^{+/+}$ (n = 8), *E4F1*$^{-/flox}$; *Ink4a/Arf*$^{+/+}$ (n = 16), *E4F1*$^{+/flox}$; *Ink4a/Arf*$^{-/-}$ (CT; n = 24), and *E4F1*$^{-/flox}$; *Ink4a/Arf*$^{-/-}$ (KO; n = 30) mice, as indicated. The arrow indicates the first 4OHT administration. The dashed lines indicate the median survival time (50% lived animals), and the double-headed arrow shows the difference in that median survival time between the two experimental groups: *E4F1* WT; *Ink4a/Arf* KO and *E4F1* KO; *Ink4a/Arf* KO. Statistically significant differences for pairwise comparison were evaluated by a log-rank test. *, P = 0.005. (B) IHC analyses of lung sections of *E4F1* CT or KO mice stained with an antibody for the Mac2 histiocytic-specific marker. Representative microphotographs at low and high magnification are shown. Bars: (left) 1 mm; (right) 100 µm. (C) Spleen weight of *E4F1* CT or KO animals. A microphotograph of spleen from a representative *E4F1* CT or KO mouse is shown. Untransplanted tumor-free mice (normal spleen) were used as controls (median ± SD; n = 17 for each group; ***, P < 0.001).

As depicted in Fig. 2 A, *E4F1* inactivation significantly increased the lifespan of animals transplanted with *Ink4a/Arf* KO cells, with a median survival time (50% survival) of 28 wk and 32 wk in *E4F1* CT and KO animals, respectively. Of note, ∼20% of *E4F1* KO; *Ink4a/Arf* KO animals exhibited a much longer lifespan, with death occurring up to 12 wk later than the last *E4F1* CT; *Ink4a/Arf* KO animal. Necropsy and histological experiments of all animals, performed at the time of their natural death, indicated that loss of *E4F1* reduced tumor infiltration in the main sites of HS dissemination, including lungs, liver, and spleen (Fig. 2 B, Fig. S2 B, and not depicted). This reduction of tumor infiltration was also illustrated by a 2.5-fold decrease of the median spleen weight (Fig. 2 C) in *E4F1* KO; *Ink4a/Arf* KO when compared with control animals.

These pathological analyses suggested that *E4F1* inactivation delayed tumor development in animals transplanted with *Ink4a/Arf* KO cells. To further confirm E4F1 impact on tumorigenesis, we set up an independent experimental group for longitudinal experiments in which tumor progression was monitored on individual animals by in vivo positron emission tomography (PET) imaging. We performed quantitative analyses on four independent animals of each genotype (*E4F1* CT or KO; *Ink4a/Arf* KO). Besides classical PET background observed in heart (Fig. S2 A) that precluded analysis of tumor development in lungs, we efficiently followed tumor progression in the liver and spleen. As expected, we observed increased PET signal in both the liver and spleen of *E4F1* CT; *Ink4a/Arf* KO animals during the time course of the experiment, illustrating the normal progression of the disease. In striking contrast, we found that *E4F1* inactivation, upon 4OHT administration to *E4F1* KO; *Ink4a/Arf* KO animals, resulted in a strong decrease of PET signal in both the liver and spleen (Fig. 3, A and B; and Fig. S2 C). Consistent with this tumor regression, we observed on tissue sections prepared from *E4F1* KO; *Ink4a/Arf* KO animals that Mac2-positive HS tumor cells exhibited increased TUNEL (terminal deoxynucleotidyl transferase biotin-dUTP nick end labeling) staining, which is a hallmark of cell death (Fig. 3 C). Altogether, these analyses revealed that *E4F1* inactivation delayed HS development, increased lifespan in this tumor-prone animal model, and induced tumor regression in established HSs.

E4F1 inactivation induced massive cell death of HS cells

Our results prompted us to analyze the cellular consequences of *E4F1* inactivation in several HS cell lines that we established from our HS murine model. Flow cytometry and immunofluorescence analyses indicated that the established cell lines expressed predominantly the Mac2 or F4/80 surface markers, with some cell lines expressing both markers, confirming their histiocytic origin (Fig. S4, A and B). Conditional *E4F1* inactivation was induced by the addition of 4OHT in the culture medium of *E4F1*$^{-/flox}$ HS cell lines (hereafter referred to as *E4F1* CT or KO, according to the absence or presence of 4OHT in the culture medium, respectively), resulting in efficient depletion of the E4F1 protein (Fig. 4 A). *E4F1* inactivation in vitro resulted in a dramatic decrease of viable cells 3 d

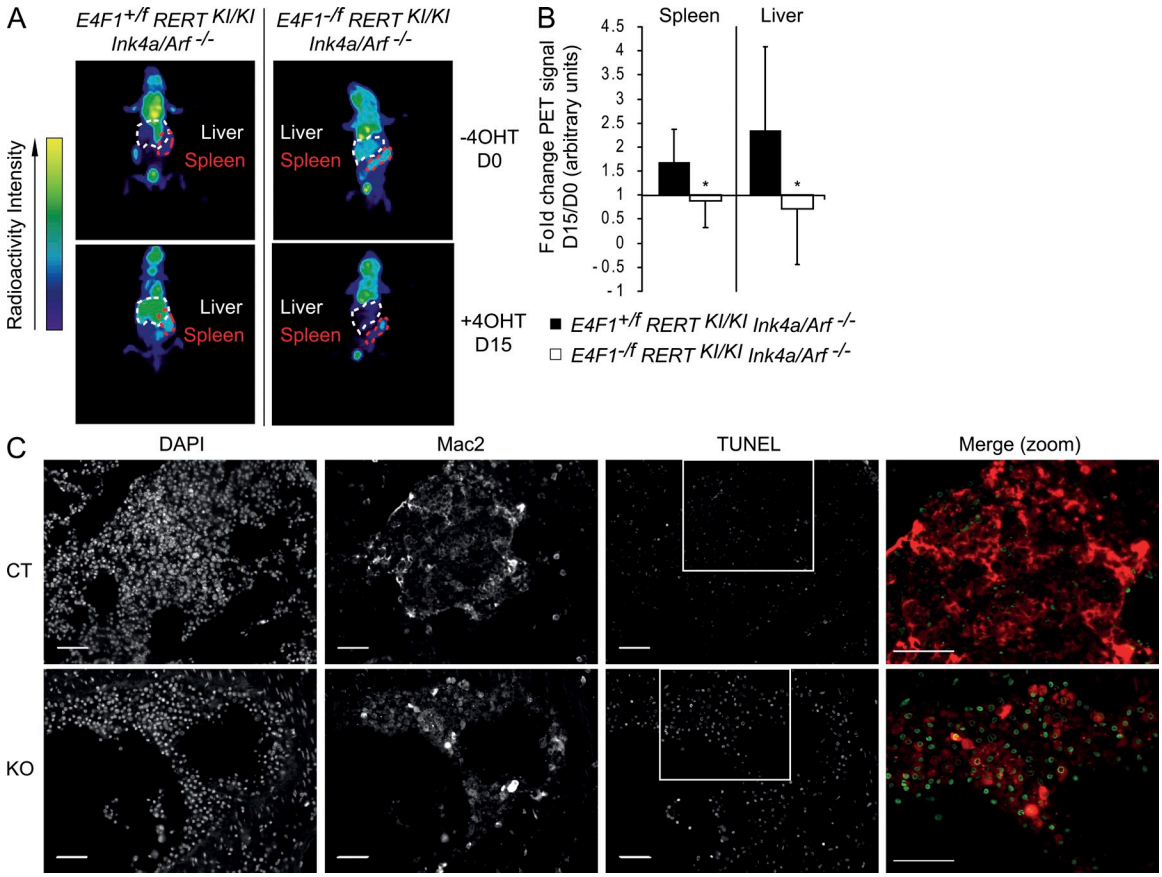

Figure 3. ***E4F1*** **inactivation results in cell death and tumor regression in established HSs.** (A and B) [^{18}F]FDG-based PET scan analyses were performed on individual *E4F1*$^{+/flox}$; *RERT*$^{KI/KI}$; *Ink4a/Arf*$^{-/-}$ and *E4F1*$^{-/flox}$; *RERT*$^{KI/KI}$; *Ink4a/Arf*$^{-/-}$ mice before (top) or 2 wk after (bottom) repeated administrations of 4OHT (n = 4 for each group). (A) Representative images showing HSs in the spleen (red dashed lines) and liver (white dashed lines). The color code indicates radioactivity intensity (arbitrary units) representing [^{18}F]FDG uptake. Note that strong PET signal in heart and pectoral muscles precluded analysis of tumor progression in the lungs. (B) Quantitative analysis of PET imaging performed on the spleen and liver (fold change representing the ratio between PET signal after 15 d [D15] and before [D0] 4OHT administration to *E4F1* CT or KO mice; median ± SD of four animals for each genotype; *, $P < 0.05$). (C) Representative microphotograph of TUNEL staining performed on lung tissue sections prepared from *E4F1*$^{+/flox}$; *RERT*$^{KI/KI}$; *Ink4a/Arf*$^{-/-}$ (CT) and *E4F1*$^{-/flox}$; *RERT*$^{KI/KI}$; *Ink4a/Arf*$^{-/-}$ (KO) mice 15 d after 4OHT administration. Sections were colabeled with TUNEL, Mac2, and DAPI, as indicated. Merge images (Mac2, red; TUNEL, green) are shown at higher magnification (boxed areas). Bars, 50 µm.

after 4OHT addition. Importantly, *E4F1*$^{+/flox}$ HS cell lines remained grossly unaffected by 4OHT treatment, confirming that the decreased number of viable cells observed in *E4F1*$^{-/flox}$ cells was not the consequence of 4OHT toxicity but resulted from E4F1 depletion (Fig. 4 A and Fig. S4 C). *E4F1* KO HS cells exhibited no alteration of their proliferation rate or of their mitotic index 4 d after 4OHT addition (Fig. 4 B). However, we observed massive cell death upon *E4F1* inactivation, as shown by increased annexin V staining (Fig. 4 C). Consistent with this result, *E4F1* inactivation abrogated the formation of colonies in anchorage-independent assays (Fig. 4 D). Altogether, these data indicated that E4F1 depletion resulted in massive cell death in murine HS cell lines established from primary tumors.

E4F1 inactivation results in autophagic cell death in HS cells

Time-lapse video microscopy analyses of *E4F1* KO HS cells showed the apparition of large vacuoles reminiscent of autophagy (unpublished data) 3–4 d after 4OHT treatment, just before cell death occurred. Autophagy is a self-degradation process implicating the lysosomal pathway in which intracellular membrane structures engulf altered organelles or aggregated proteins. We sought additional experimental evidences of autophagy in *E4F1* KO HS cells by several complementary approaches. Transmission electron microscopy indicated the presence of ultrastructural characteristics of autophagic cells, such as double-membraned autophagosomes and autolysosomes, in *E4F1* KO HS cells (Fig. 5 A). Moreover, we observed by immunoblot that *E4F1* inactivation resulted in the conversion of cytoplasmic LC3 (LC3-I) protein to the autophagosome membrane-bound form of LC3 (LC3-II), which is a hallmark of autophagy (Fig. 5 B). Finally, increased formation of autophagosomes and autolysosomes in *E4F1* KO HSs was visualized by fluorescence microscopy after anti-LC3 or acridine orange (AO) stainings, respectively (Fig. 5, C and D).

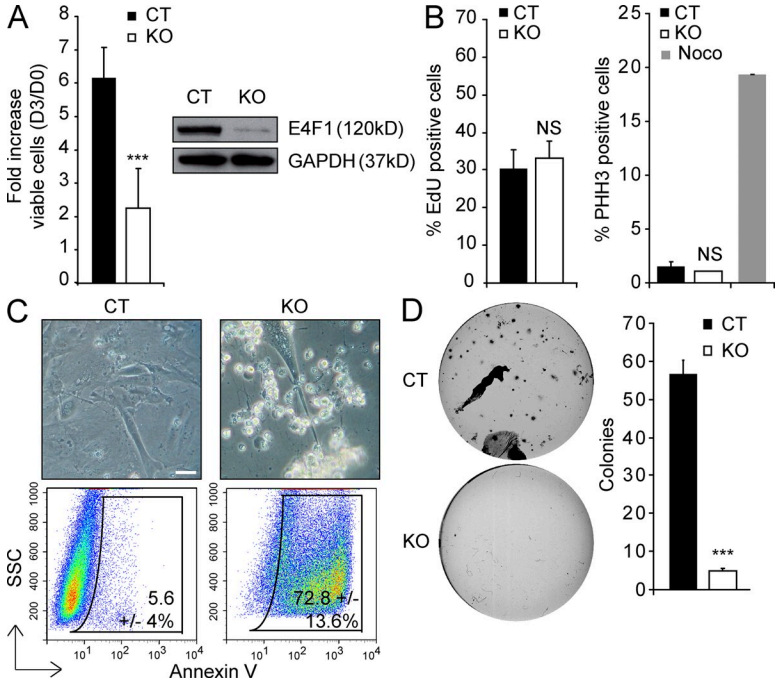

Figure 4. *E4F1* inactivation induces massive cell death of HS cells. *E4F1*$^{-/flox}$; *RERT*$^{KI/KI}$; *Ink4a/Arf*$^{-/-}$ HS cells were cultured in the presence (KO) or absence (CT) of 4OHT. (A) 3 d after vehicle or 4OHT addition in the culture medium, HS cells were analyzed by immunoblot and counted (mean ± SD; $n = 6$; ***, $P < 0.001$). GAPDH was used as a loading control. (B) Proliferation rate and mitotic index upon *E4F1* inactivation in HS cells. The percentage of EdU (left)- or phosphohistone H3 (S10; PHH3; right)–positive cells was evaluated by flow cytometry. Nocodazole treatment (Noco) of *E4F1* CT HS cells was used as a control for PHH3 staining. Bar graphs represent the mean ± SD ($n = 3$). (C) Representative microphotographs (top) of *E4F1* CT and KO HS cells 4 d after 4OHT addition. Flow cytometry analyses (bottom) of annexin V–positive cells in *E4F1* CT and KO HS cells (numbers indicate the mean ± SD of $n = 7$; $P < 0.001$). Bar, 5 µm. (D) 10^5 *E4F1* CT and KO HS cells were seeded in soft agar. Bar graph shows quantitative evaluation of the total number of colonies formed after 3 wk of culture (mean ± SD; $n = 3$; ***, $P < 0.001$).

To determine whether induction of autophagy was the main cause of *E4F1* KO HS cell death, cells were treated with the autophagy inhibitor 3-methyladenine (3MA), which blocks an early step controlling autophagosome formation (Levine and Kroemer, 2008; Mizushima, 2009). 3MA efficiently blocked autophagy and cell death in *E4F1* KO cells, as shown by decreased LC3-II expression and reduced number of annexin V–positive cells (Fig. 5, B and E). We also evaluated whether apoptosis contributed to cell death occurring upon *E4F1* inactivation. The z-VAD caspase inhibitor had a minor but significant effect on cell death of *E4F1* KO HS cells (Fig. S5 A). Altogether, these results showed that *E4F1* KO HS cells died mainly through autophagic cell death with a minor implication of apoptosis.

Autophagic cell death of E4F1 KO HS cells results from mitochondrial defects and increased reactive oxygen species (ROS) levels

Oxidative stress is a well-known inducer of autophagy in a variety of cell types including macrophages (Xu et al., 2006). Therefore, we wondered whether autophagy observed in *E4F1* KO HS cells resulted from increased ROS levels. *E4F1* KO HS cells exhibited increased staining with the 2′,7′-dichlorofluorescein diacetate (DCFDA) probe, a cell-permeable fluorescent dye that reacts with a broad spectrum of ROS (Fig. 6 A). Importantly, DCFDA staining in *E4F1* KO HSs was not modified by the autophagy inhibitor 3MA, indicating that increased ROS levels resulting from *E4F1* inactivation were not a consequence of autophagic cell death (Fig. S6 A). Consistent with the development of an early and massive oxidative stress in these cells, a robust antioxidant response was detectable early after *E4F1* inactivation, as illustrated by an increased expression of several antioxidants factors, including the transcription factor NRF2, catalase, HO1 (heme oxygenase 1), and NQO1 (NAD[P]H dehydrogenase quinone 1; Fig. S6, C–F).

Incubation with probes that detect specific ROS subtypes such as MitoSOX and OxyBURST confirmed that the oxidative stress that resulted from *E4F1* inactivation included increased levels of superoxide anions of mitochondrial origin (Fig. 6 A). These data suggested that this organelle could be the main source of ROS detected in *E4F1* KO HS cells. As a read-out of potential mitochondrial alterations in *E4F1* KO HS cells, we next determined their in situ oxygen consumption rates (OCRs) and ATP levels. Compared with control cells, *E4F1* KO HS cells exhibited a strong increase in O_2 consumption (at all levels, i.e., basal respiration, oligomycin C–sensitive respiration, and maximum respiratory capacity; Fig. 6 B). Strikingly, this strong increase in mitochondrial O_2 consumption was not associated with efficient ATP production because *E4F1* KO HS cells exhibited decreased ATP levels (Fig. 6 C). Because it is well established that various alterations of the electron transport chain functions increase ROS production (Koopman et al., 2010), this strongly suggests that *E4F1* KO HS cells display mitochondrial alterations that impinge on the efficient coupling between oxygen consumption and ATP production, ending in increased ROS production.

The direct consequence of a massive increase in ROS levels is the oxidation of the cellular components, including DNA. Accordingly, we detected increased levels of 8-hydroxy-2′-deoxyguanosine (8-OHdG) in *E4F1* KO HS cells, which is a stable marker of oxidatively damaged DNA, as shown by nuclear relocalization and increased intensity of the 8-OHdG staining (Fig. 6 D; Struthers et al., 1998).

These data led us to further investigate whether these ROS were the main cause of death that resulted from *E4F1* inactivation. Treatment of *E4F1* KO HS cells with the superoxide anion scavenger Tiron (4,5-dihydroxy-1,3-benzene disulfonic acid-disodium salt) (a) resulted in reduction of the conversion of LC3-I to LC3-II (Fig. 6 E), (b) diminished

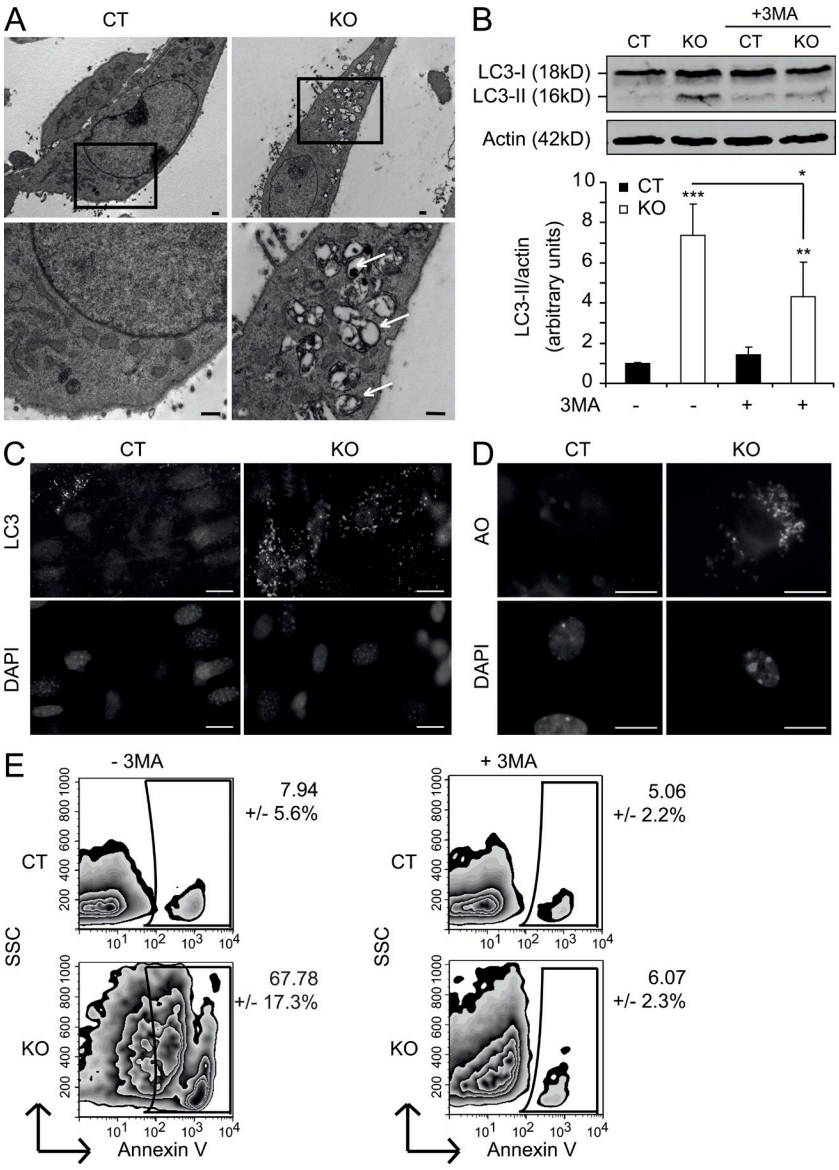

Figure 5. *E4F1* inactivation in HS cells results in autophagic cell death. *E4F1*$^{-/flox}$; *RERT*$^{KI/KI}$; *Ink4a/Arf*$^{-/-}$ HS cells were cultured in the presence (KO) or absence (CT) of 4OHT. (A) Representative microphotographs of electron microscopy analyses showing the formation of autophagic vacuoles in *E4F1* KO HS cells (top). Higher magnification (bottom) of the same cells (boxed areas) showing the apparition of double-membraned cytoplasmic vacuoles containing dark degradation products in *E4F1* KO HS cells (white arrows). (B) Quantitative immunoblot analyses of conversion of LC3-I to LC3-II upon *E4F1* inactivation in HS cells. Treatment with the autophagy inhibitor 3MA is indicated. Actin was used as a loading control. Top panels show representative immunoblots. The bottom panel represents the quantitative analyses of LC3-II levels normalized to actin levels (mean ± SD; $n = 3$; *, $P < 0.05$; **, $P < 0.01$; ***, $P < 0.001$). (C) Representative microphotograph of HS cells stained with anti-LC3 antibody and DAPI and visualized by fluorescence microscopy. (D) Formation of acidic vesicular organelles in HS cells was visualized by fluorescence microscopy after staining with the lysosomal-specific dye AO and DAPI. (E) Percentage of annexin V–positive HS cells was measured by flow cytometry (mean ± SD; $n = 3$). Cells were treated with 3MA where indicated. Bars: (A) 500 nm; (C and D) 10 µm.

nuclear labeling of 8-OHdG (Fig. 6 D), (c) and led to a marked decrease in the number of annexin V–positive cells (Fig. S5 B). Similar results were obtained with 3H-1,2 dithiole-3-thione (D3T), a chemical compound which increases cellular antioxidant defenses by increasing NRF2 activities (Fig. 6 E and Figs. S5 B and S6 H; Zhu et al., 2006). In addition, treatment of *E4F1* KO HS cells in culture with the ROS scavenger *N*-acetyl-L-cysteine (NAC) rescued cellular viability 3 d after 4OHT addition (Fig. 7 A). Finally, NAC treatment of *E4F1* KO; *Ink4a/Arf* KO animals strongly altered the massive cell death occurring in established HSs upon *E4F1* inactivation in vivo, as shown by decreased TUNEL staining performed on tissue sections prepared from these animals (Fig. 7, B and C). Collectively, our data support the notion that *E4F1* inactivation in HS cells results in mitochondrial defects and oxidative stress that lead to autophagic cell death, both in vitro and in vivo.

Increased ROS levels and cell death do not occur in E4F1 KO primary normal macrophages

Careful monitoring of *E4F1* KO or CT; *Ink4a/Arf* WT animals indicated that E4F1 depletion did not dramatically affect the different lymphoid and myeloid populations in the peripheral blood (not depicted) and did not alter the lifespan of those animals over a 12-mo observation period in that experimental setting (Fig. 2 A). Therefore, we investigated whether cell death resulting from *E4F1* inactivation in HS cells was specific of transformed cells. To address this question, we inactivated *E4F1* ex vivo in purified intraperitoneal primary murine macrophages. Although efficient *E4F1* depletion was obtained upon 4OHT addition ex vivo, neither increased oxygen consumption, increased ROS levels, nor induced cell death were detected in these cells (Fig. 8). These data showed that *E4F1* inactivation resulted in cell death selectively in transformed cells originating from the monocytic/macrophagic lineage but not in normal primary macrophages.

E4F1 depletion results in mitochondrial defects, increased ROS levels, and cell death in human myeloid tumor cells

The consequences of E4F1 depletion in HS cell survival prompted us to evaluate whether the observed defects could be extended to human leukemic cell lines of myeloid origin. We first evaluated the consequences of E4F1 depletion in

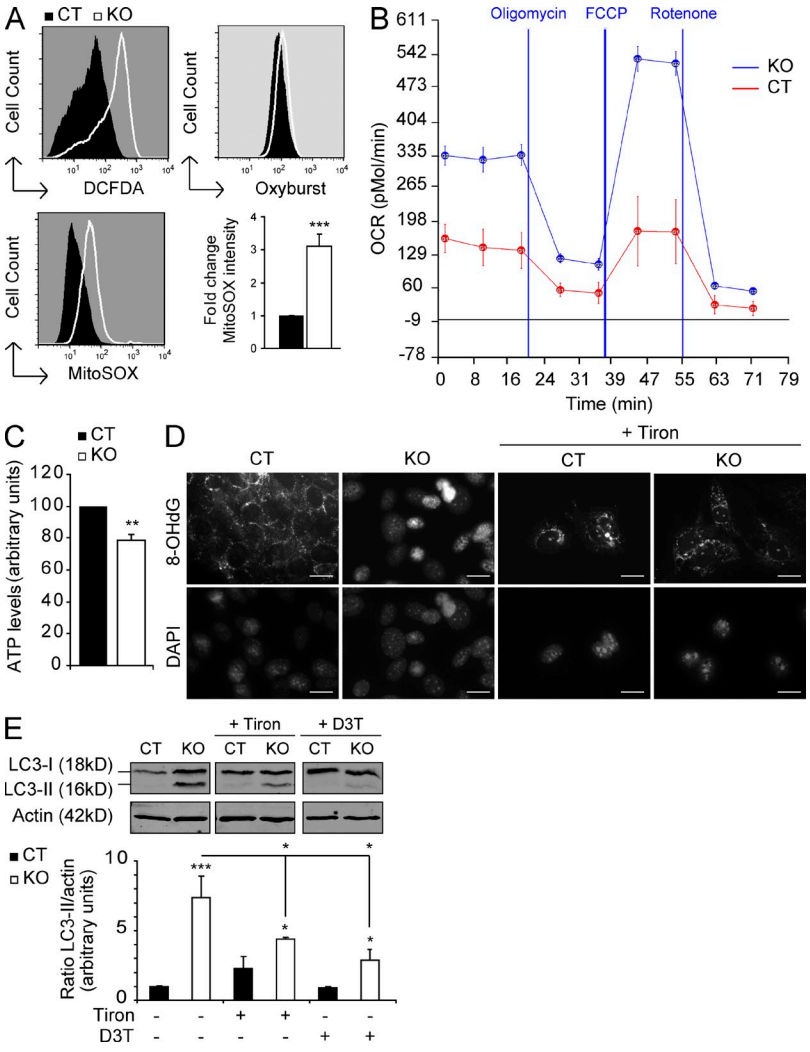

Figure 6. *E4F1* inactivation results in mitochondrial defects and increased ROS levels. *E4F1*$^{-/flox}$; *RERT*$^{KI/KI}$; *Ink4a/Arf*$^{-/-}$ HS cells were cultured in the presence (KO) or absence (CT) of 4OHT. (A) Flow cytometry analyses of ROS levels measured by DCFDA, OxyBURST, and the mitochondria-specific MitoSOX probes in *E4F1* CT and KO HS cells, as indicated. Bar graph represents quantitative data showing fold increase of time-dependent changes in mean fluorescence intensity of MitoSOX measured by flow cytometry (mean ± SD; $n = 3$; ***, $P < 0.001$). (B) Mitochondrial OCR corresponding to basal respiration, oligomycin-sensitive OCR, and maximal respiration (evaluated upon injection with the uncoupling agent FCCP followed by the inhibitor of the mitochondrial complex I rotenone) in HS cells, as indicated. Values were normalized to total protein levels. Vertical bars indicate the time of injection of the indicated compound. Data are represented as the mean ± SD of triplicate experiments. (C) Total ATP levels in *E4F1* CT and KO HS cells were measured 3 d after 4OHT addition (mean ± SD; $n = 3$; **, $P < 0.01$). (D) Genomic DNA oxidation was measured in HS cells by fluorescent microscopy using a direct binding assay based on avidin-conjugated FITC that binds 8-OHdG, in the presence or absence of the superoxide anion scavenger Tiron. Representative images of three independent experiments are shown. Bars, 10 µm. (E) Quantitative immunoblot analyses of LC3 expression in total protein extracts prepared from *E4F1* CT and KO HS cells treated with vehicle, Tiron, or D3T, an inducer of cellular antioxidant defenses, as indicated. LC3-II levels were normalized to actin levels (mean ± SD; $n = 3$; *, $P < 0.05$; ***, $P < 0.001$).

U937 cells, a cell line originally isolated from pleural effusion of a patient with HSs (Sundström and Nilsson, 1976). E4F1 depletion was achieved by transduction of cells with lentiviruses encoding two independent short hairpin RNAs (shRNAs) directed against human E4F1 or a control irrelevant shRNA (Fig. 9 A). E4F1 depletion in U937 cells resulted in increased ROS levels. Comparable results were obtained in other leukemic cell lines, including the acute promyelocytic leukemia HL60, the acute monocytic leukemia THP1, and the erythroleukemic HEL cell lines (Fig. 9 B and Fig. S8 D). Interestingly, similar to murine HS cells, E4F1 depletion in HEL and HL60 cells resulted in increased oxygen consumption (Fig. 9 C). These defects led to massive cell death, as shown by increased annexin V staining (Fig. 9 D).

Altogether, our data suggest that the essential roles of E4F1 in mitochondrial functions and cell survival observed in murine HS cells extend to human leukemic cell lines. Based on this conclusion, we next conducted a pilot experiment aimed at evaluating E4F1 expression levels in samples isolated from leukemic patients.

E4F1 is overexpressed in a large subset of primary human AML samples

HS is a rare human tumor precluding the analysis of a significant number of samples. Because we found that E4F1 depletion induced comparable defects in several leukemic cell lines of myeloid origin, we evaluated E4F1 expression levels in AML, a more common myeloid malignancy. E4F1 protein level was assessed by quantitative immunoblotting on protein extracts prepared from 39 BM biopsies harvested from patients diagnosed with AML. Normal BM samples were used as controls. The vast majority (35/39) of AML expressed E4F1 at higher levels than controls, with a subgroup (9/39) that we defined as strong overexpressors (4–13-fold increase above controls; Fig. 9 E and Fig. S8 C). These data were consistent with our observation that murine HS cell lines exhibit a higher amount of E4F1 messenger RNA (mRNA) and protein levels compared with primary macrophages (Fig. S8, A and B). Thus, this pilot experiment suggested that leukemic cells overexpress E4F1 protein, which is consistent with the notion that E4F1 is essential for their survival.

DISCUSSION

Although the multifunctional E4F1 protein is involved in essential oncogenic pathways, its exact functions during transformation remain poorly understood. In this study, we

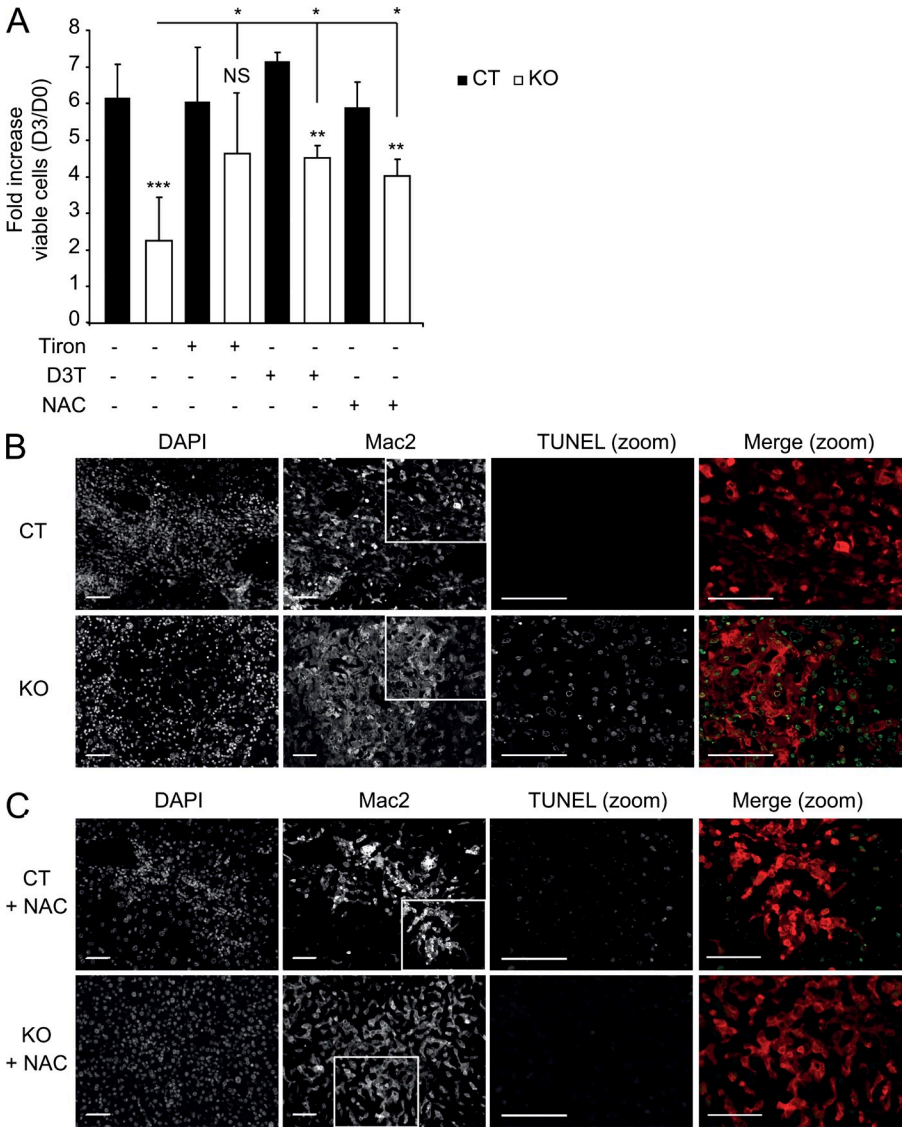

Figure 7. ROS scavengers rescue cell death occurring in *E4F1* KO HS cells. (A) *E4F1*$^{-/flox}$; *RERT*$^{KI/KI}$; *Ink4a/Arf*$^{-/-}$ HS cells were cultured in the presence (KO) or absence (CT) of 4OHT. Number of viable cells assessed in the absence or presence of the ROS scavengers Tiron or NAC or upon the addition of D3T in *E4F1* KO or CT HS cells, as indicated. Bar graph represents quantitative analysis showing fold increase of viable HS cells between days 0 (D0) and 3 (D3) after 4OHT treatment (mean ± SD; $n = 3$; *, $P < 0.05$; **, $P < 0.01$; ***, $P < 0.001$). (B and C) Representative microphotographs of TUNEL staining performed on liver tissue sections prepared from vehicle (B)- or NAC (C)-treated *E4F1*$^{+/flox}$; *RERT*$^{KI/KI}$; *Ink4a/Arf*$^{-/-}$ (CT) or *E4F1*$^{-/flox}$; *RERT*$^{KI/KI}$; *Ink4a/Arf*$^{-/-}$ (KO) mice 15 d after 4OHT administration. Sections were colabeled with TUNEL, Mac2, and DAPI as indicated. Merge images (Mac2, red; TUNEL, green) are shown at higher magnification (boxed areas). Bars, 50 µm.

evaluated *E4F1* functions in tumor development in vivo, using an original mouse model based on mice transplanted with genetically engineered HSCs harboring *Ink4a/Arf*-null and *E4F1* conditional KO alleles. This strategy resulted in the generation of a tumor-prone mouse model with unexpected tumor spectrum. Although other murine models based on the *Ink4a/Arf* KO allele have previously been shown to develop mainly lymphomas and sarcomas (Serrano et al., 1996), we failed to detect any pathological evidences of lymphoma development in our transplanted mice. The absence of lymphoma in our experimental model did not reflect differences in genetic backgrounds because genetically matched donor mice developed lymphomas with the expected frequency (Fig. S1 E). Strikingly, all of our transplanted mice developed HSs, a rare neoplasm of the histiocytic lineage with poor prognosis and aggressive clinical course in humans. Most human HS cases previously described were originally misclassified and are now recognized as diffuse large B cell lymphomas with associated reactive macrophages. However, extensive morphological and immunophenotypical analyses confirmed that the hematopoietic tumors arising in our model are bona fide HSs, according to criteria published in the World Health Organization classification of human tumors. The high penetrance of this tumor type raised the question about the molecular etiology and cell of origin of HSs. Consistent with previous studies, our data support the cooperating role of functional alterations of the *Ink4a/Arf* locus and the phosphoinositide 3-kinase (PI3K) pathway in HS pathogenesis in murine models (Eischen et al., 2002; Lund et al., 2002; Carrasco et al., 2006). Indeed, although PTEN protein remained expressed in all HS cell lines established from our murine model, we found clear evidence for a deregulation of the PI3K pathway, as illustrated by a marked increase in the activating phosphorylation of AKT on Ser473 (Fig. S3). Because only few relevant HS mouse models exist so far (Martín-Caballero et al., 2001; Eischen et al., 2002; Carrasco et al., 2006; Khoo et al., 2007), the characterization of this new model exhibiting full penetrance and apparent specificity for the development of HS might help to better understand the etiology of this aggressive disease.

Using this tumor-prone mouse model, we found that *E4F1* inactivation resulted in the massive cell death of transformed cells, tumor regression, and increased life span of the transplanted animals. Nevertheless, *E4F1* KO; *Ink4a/Arf* KO animals still died earlier than *E4F1* KO; *Ink4a/Arf* WT mice.

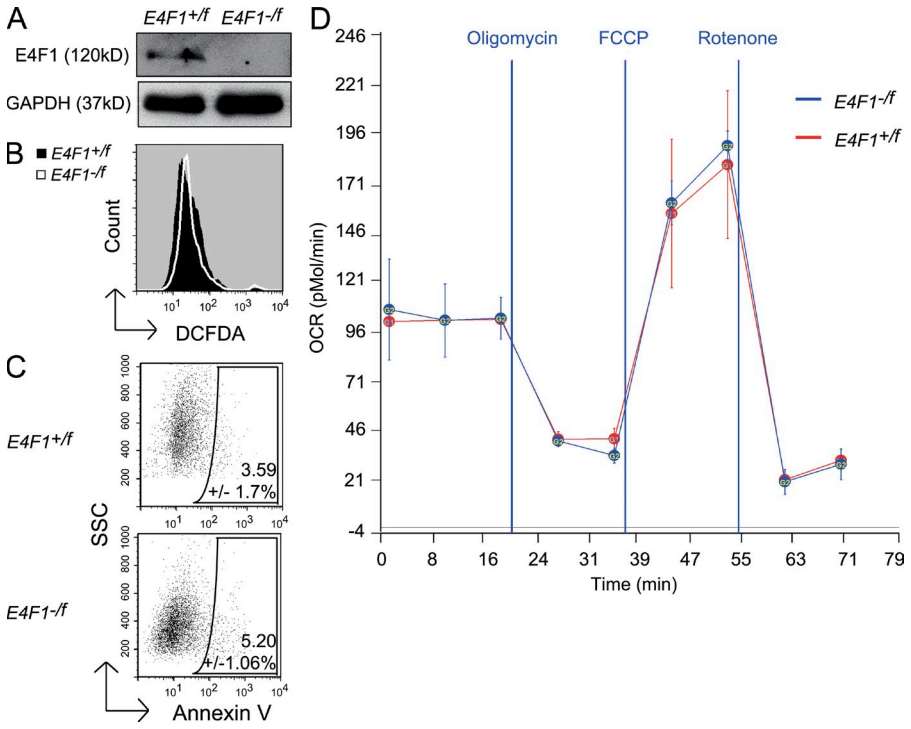

Figure 8. *E4F1* inactivation does not result in mitochondrial defects, increased ROS levels, or increased cell death in normal primary macrophages. Primary macrophages were purified from the intraperitoneal cavity of age-matched *E4F1*$^{+/flox}$; *RERT*$^{KI/KI}$ or *E4F1*$^{-/flox}$; *RERT*$^{KI/KI}$ animals. *E4F1* inactivation was induced ex vivo by the addition of 4OHT in the culture medium. Analyses were performed between 4 and 5 d after 4OHT addition. (A) Immunoblot analysis of E4F1 expression in *E4F1*$^{+/flox}$ or *E4F1*$^{-/flox}$ primary macrophages. GAPDH was used as a loading control. (B) Flow cytometry analysis of intracellular ROS levels (DCFDA) in *E4F1 E4F1*$^{+/flox}$ or *E4F1*$^{-/flox}$ primary macrophages. (C) Primary macrophages were stained with annexin V and analyzed by flow cytometry. (D) OCRs of *E4F1*$^{+/flox}$ or *E4F1*$^{-/flox}$ primary macrophages were measured as described in Fig. 6. Vertical bars indicate the time of injection of the indicated compound. Data are represented as the mean ± SD of triplicate experiments.

The cause of death of these animals remains unclear. Our data do not support the idea that *E4F1* inactivation induced severe hematopoietic defects compromising the lifespan of those transplanted animals. Detailed necropsy analyses performed with trained pathologists indicated that some but not all *E4F1* KO; *Ink4a/Arf* KO animals exhibited lesions that could reflect massive and rapid cell death of tumor cells in essential organs such as lungs and liver. These defects may have resulted in a severe tissue disorganization and animal death.

To decipher *E4F1* functions in HS cell survival, we next performed extensive analyses in established HS cell lines derived from our animal models. Our previous study indicated that *E4F1* KO embryos display mitotic progression defects followed by cell death at the peri-implantation stage, as illustrated by increased mitotic index and aberrant mitotic figures (Le Cam et al., 2004). Such defects were not observed in HS cells upon acute inactivation of *E4F1*, suggesting that *E4F1* has different functions in various cell types.

Compelling evidence indicates that *E4F1* inactivation in HS cell lines turned on a switch toward autophagic cell death, a process which likely reflects the well documented propensity of cells originating from the macrophage lineage to undergo autophagy in stress conditions (Xu et al., 2006; Huang et al., 2009). Seeking the stress that had initiated this response, we found that acute *E4F1* inactivation in HS cells led to mitochondrial defects and increased ROS levels. Importantly, rescue experiments based on ROS scavengers or chemical compounds that increase cellular antioxidant defenses indicated that these ROS preceded the autophagic cell death response in *E4F1* KO HS cells. Increased ROS levels observed in these cells likely resulted in deleterious oxidation of many cellular constituents, including proteins, DNA, and lipids. Accordingly, we observed that *E4F1* inactivation in HS cells associated with massive genomic DNA oxidation that was largely abrogated upon treatment with ROS scavengers. Furthermore, administration of NAC to *E4F1* KO *Ink4a/Arf* KO animals prevented the massive cell death that was observed in vivo upon *E4F1* inactivation in established HSs. Preliminary analyses performed by PET scan on a limited number of NAC-treated animals also suggested that ROS scavengers prevented tumor regression induced by *E4F1* inactivation (unpublished data).

Those results raised the question about the source of ROS production in *E4F1* KO HS cells. Because E4F1 has been described as an interactor and a regulator of the tumor suppressor p53 (Le Cam et al., 2006), one possibility was that E4F1 depletion had modified some p53 functions leading to increased ROS levels and/or activation of an autophagic response. Indeed, beside its well documented functions on cell cycle and apoptosis, p53 has been recently shown to directly modulate DRAM (damage-regulated autophagy modulator), a component of the autophagic machinery (Crighton et al., 2006). Furthermore, transcriptional independent activities of cytoplasmic p53 have also been proposed to regulate autophagy (Tasdemir et al., 2008). Finally, p53 has been described to mediate pro- as well as antioxidant effects, likely depending on the intensity of the p53 response. Paradoxically, both have been suggested to participate in its tumor suppressor functions (Vousden and Ryan, 2009). We currently do not favor the hypothesis that activation of p53 is involved in increased ROS levels found in *E4F1* KO HS cells because those cells already harbor an altered p53 pathway resulting from genetic inactivation of the *Ink4a/Arf* locus. In addition, shRNA-mediated depletion of endogenous p53 failed to modulate

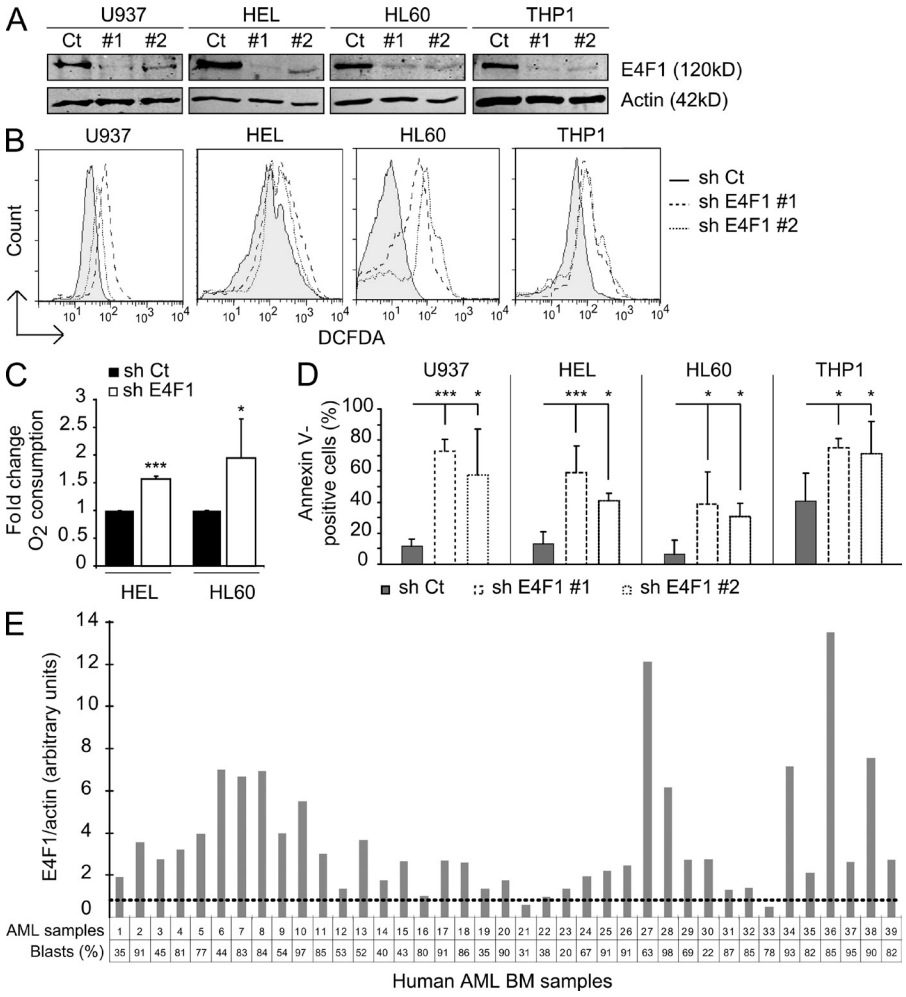

Figure 9. E4F1 is overexpressed in human AML samples, and its depletion induces mitochondrial defects, increased ROS levels, and cell death in human myeloid leukemic cell lines. (A) Immunoblot analysis of E4F1 expression in human HS U937, erythroleukemic HEL, promyelocytic leukemia HL60, and acute monocytic leukemia THP1 cell lines transduced with lentiviruses encoding two independent shRNAs (#1 and #2) directed against human E4F1 or a control irrelevant shRNA (Ct). (B) Representative flow cytometry analyses of ROS levels (DFCDA) in U937, HEL, HL60, and THP1 cell lines treated with Ct or E4F1 shRNA. (C) O_2 consumption in human HEL and HL60 myeloid leukemic cell lines upon treatment with Ct or E4F1 shRNA, as indicated. O_2 consumption was measured using a Clark-type O_2 electrode chamber. Bar graph represents the mean ± SD ($n = 3$; *, $P < 0.05$; ***, $P < 0.001$). (D) Flow cytometry analyses of annexin V–positive cells in human myeloid leukemic cell lines treated with Ct or E4F1 shRNAs (#1 and #2), as indicated. Bar graph represents the mean ± SD ($n = 3$; *, $P < 0.05$; ***, $P < 0.001$). (E) E4F1 and actin (loading control) protein expression levels were evaluated by quantitative immunoblotting on total protein extracts prepared from BM samples from adult AML patients. Bar graph represents the ratio between E4F1 and actin protein levels of individual patients. The dotted line represents the mean value of this ratio obtained with three normal BM samples. The percentage of myeloid leukemic blasts in each sample was evaluated to avoid potential bias based on heterogeneity of the AML BM samples tested.

increased ROS levels or cell death in *E4F1* KO HS cells (Fig. S7). Our data rather point to a more direct role of E4F1 in the regulation of mitochondrial activities that impinge on ROS levels. Indeed, increased ROS levels were detected by several ROS-sensitive fluorescent probes, including dyes that detect superoxide anions of mitochondrial origin. Our data support the importance of superoxide anions as a byproduct of mitochondrial defects in the induction of cell death observed in *E4F1* KO HS cells. Consistent with that notion, we found that *E4F1* inactivation resulted in perturbed mitochondrial oxygen consumption and decreased ATP production, and cell death was partly rescued upon treatment with Tiron, which allows detoxification of superoxide anions into less toxic ROS. This is of particular interest in light of our recent data showing that *E4F1* inactivation in murine fibroblasts perturbed expression of several mitochondrial components involved in energetic and metabolic processes (unpublished data). These data support the notion that high ROS levels in *E4F1* KO cells are the direct consequence of mitochondrial dysfunctions, which in turn induce cell death in HS cells. Furthermore, shRNA-mediated depletion of E4F1 in several human transformed cell lines of myeloid origin resulted in the same sequence of events, suggesting that the role of *E4F1* in those processes is conserved in murine and human leukemic cells.

The role of ROS in tumorigenesis remains controversial. On one hand, many studies describe ROS as inducers of tumorigenesis (Klaunig et al., 2010; Ziech et al., 2011). On the other hand, previous data have also shown that some cancer cells, including leukemic cells, are more sensitive to increased ROS levels than their nontransformed counterparts, opening a window of opportunity for pro-oxidant anticancer treatments (Huang et al., 2000; Trachootham et al., 2006, 2008; Valko et al., 2007). Our data are consistent with the latter strategy because we found that *E4F1* inactivation induces ROS-mediated cell death in HS transformed cells but not in normal primary macrophages. The molecular mechanisms that are responsible for the higher sensitivity of cancer cells to increased ROS levels still remain unclear. Several explanations have been proposed, implicating the lower antioxidant defenses in some tumor cells or the paradoxical role of AKT in sensitizing cancer cells to ROS-induced cell death (Huang et al., 2000; Nogueira et al., 2008). Based on our data showing that transformed but not normal cells display mitochondrial

defects upon E4F1 depletion, we also do not exclude the possibility that transformed cells exhibit deregulation of some yet unidentified mitochondrial activities that sensitize cancer cells to E4F1 depletion. Together with our finding that overexpression of E4F1 protein level, ranging from moderate (two- to fourfold) to high (4–13-fold), occurs in a large subset of AML samples, these observations raise an interesting hypothesis that some leukemic cells become addicted to the prosurvival functions of E4F1 during the process of cell transformation. In conclusion, our findings may have important implications for novel anticancer therapies, in particular for treatment of leukemias that have been shown to respond to chemotherapeutic agents that regulate the redox status.

MATERIALS AND METHODS

Generation of mutant mice and *E4F1* inactivation in vivo. *E4F1*-null and *E4F1*^{flox} mice were generated previously (Le Cam et al., 2004; Lacroix et al., 2010). *Ink4a/Arf* (Serrano et al., 1996) and *RERT* (Guerra et al., 2003) mice were provided by M. Serrano and M. Barbacid (Centro Nacional de Investigaciones Oncológicas, Madrid, Spain), respectively. *E4F1*-null, *E4F1*^{flox}, *RERT*, and *Ink4a/Arf* mice were intercrossed to obtain appropriate genotypes: *E4F1*$^{+/flox}$ or *E4F1*$^{-/flox}$; *RERT*$^{KI/KI}$; *Ink4a/Arf*$^{+/+}$ or *Ink4a/Arf*$^{-/-}$. The mice were maintained on a mixed 129Sv/J/DBA/C57BL/6 background. *E4F1*^{flox}; *RERT* mice were genotyped by PCR on tail genomic DNA using the following primers. (a) E4F1 WT (*E4F1*$^{+}$) and conditional KO flox alleles (*E4F1*^{flox}): 5′-CCTTGAGCACGGAGGAGAGC-3′ and 5′-GCCCTAGCCTGCTCTGCCATC-3′. (b) *E4F1* constitutive KO allele (*E4F1*$^{-}$): 5′-CACTGCCTTGGAGGACTTTG-3′ and 5′-CCTCTGTTCCACATACACTTCATTC-3′. (c) WT and KI *RERT* alleles: 5′-GTCAGTACACATACAGACTT-3′, 5′-TGAGCGAACAGGGCGAA-3′, and 5′-TCCATGGAGCACCCAGTGAA-3′. (d) *Ink4a/Arf* alleles: WT, 5′-ATGATGATGGGCAACGTTC-3′ and 5′-CAAATATCGCACGATGTC-3′; and KO, 5′-CTATCAGGACATAGCGTTGG-3′ and 5′-AGTGAGAGTTTGGGGACAGAG-3′.

In vivo recombination of the *E4F1*^{flox} allele was obtained by topical skin applications of 4OHT (Sigma-Aldrich) on shaved back skin of the transplanted recipient animals (2 mg/mouse/application; three applications). Cre-mediated *E4F1* recombination efficiency was assessed by immunoblotting or by qPCR analysis on genomic DNA using primers specific for the *E4F1* locus, as described in Fig. S1 A: primer A, 5′-GGCTGCTGCGTGGATTTC-3′; B, 5′-GCTAGGTAGGGTAGGAGGCTGTCT-3′; C, 5′-TTCGGTATAGTGTTGAGG-3′; and D, 5′-AGGGGCTGGGCTACAATGG-3′.

For survival analyses, 4OHT administration started 10 wk after transplantation and was repeated on a monthly basis throughout the entire life of the animals. For PET scan analyses, 4OHT (2 mg/mouse/application; three applications) was administrated around 20 wk after transplantation, when animals exhibited obvious signs of tumor development. For NAC-based in vivo experiments, NAC was administrated at the final concentration of 40 mM in the drinking water (changed every day) for 7 d before 4OHT administration and maintained afterward during the total duration of the experiment (15 d). All animal husbandry and experiments were approved by and performed in accordance with the guidelines of the Institute of Molecular Genetics Ethics Committee (agreement no. B-34-172-16).

Transplantation experiments. Congenic C57BL/6-Ly5.1 mice were lethally irradiated (11 Gy) with a cobalt radiation source and used as recipient mice. 5 × 10^6 fetal liver donor HSCs isolated from Ly5.2 *E4F1*$^{-/flox}$ or *E4F1*$^{+/flox}$; *RERT*$^{KI/KI}$; *Ink4a/Arf*$^{+/+}$ or *Ink4a/Arf*$^{-/-}$ embryonic day (E) 14.5 embryos, were injected i.v. into the tail vain of recipient (Ly5.1) mice. Peripheral blood was obtained from retroorbital sinuses of recipient mice under isoflurane anesthesia and analyzed every 4 wk after transplantation by flow cytometry with several combinations of lineage-specific antibodies: APC-CD19 for B cells, PerCP-CD3 for T cells, and APC-Gr1, FITC-F4/80, or PE-Mac2 for myeloid cells. PE-CD45.1 (Ly5.1) and FITC-CD45.2 (Ly5.2) antibodies were used to determine the level of reconstitution by identifying the proportion of donor cells in recipient mice. Fluorochrome-conjugated antibodies used for flow cytometry analyses (FACSCalibur flow cytometer; BD) were purchased from BD and eBioscience. Flow cytometry data were analyzed with FlowJo software (Tree Star).

RT-qPCR. *E4F1* mRNA expression was evaluated in different hematopoietic compartments by RT-PCR. Cells were lysed in TRIZOL reagent (Invitrogen), and total RNAs were isolated according to the manufacturer's recommendations. cDNAs were synthesized from 1 µg of total RNA using random hexamers and SuperScript III Reverse transcription (Invitrogen). Real-time qPCR was performed on a LightCycler 480 SW 1.5 apparatus (Roche) with Platinum Taq DNA polymerase (Invitrogen) and an SYBR Green mix containing 3 mM $MgCl_2$ and dNTPs 30 µM each; 45 cycles of 95°C for 4 s, 62°C for 10 s, and 72°C for 30 s. Results were quantified with a standard curve generated with serial dilutions of a reference cDNA preparation. PCR products were always loaded on an agarose gel to verify fragment size and purity of amplicons. *RPL13A* and *HPRT* transcripts were used for normalization. Primers sequences were as follows: *E4F1* forward, 5′-CCAAAGCCTACCTGCTCAAG-3′; and reverse, 5′-CTGGGCATTCTTGGTTTTGT-3′; *RPL13A* forward, 5′-GAGGTCGGGTGGAAGTACCA-3′; and reverse, 5′-TGCATCTTGGCCTTTTCCTT-3′; and *HPRT* forward, 5′-AAGCCTAAGATGAGCGCAAG-3′; and reverse, 5′-TTACTAGGCAGATGGCCACA-3′.

Histology and immunohistochemistry (IHC). Formalin-fixed tissues were embedded in paraffin, sectioned, and processed for routine hematoxylin and eosin (H&E) staining and IHC. Anti-Ki67 (SP6) and -MPO (Ab-1) antibodies were obtained from Thermo Fisher Scientific. Anti–CD3-ε (M-20) and -Pax5 (C-20) antibodies were obtained from Santa Cruz Biotechnology, Inc., and anti-F4/80 (BM8) and -Mac2 (M3/38) antibodies were obtained from eBioscience. IHC was performed on 4-µm tissue sections using the appropriate primary antibodies and the corresponding biotinylated secondary antibody coupled to streptavidin–peroxidase complex (ABC Vectastain kit; Vector Laboratories). Revelation was performed using the peroxidase substrates DAB (3,3′-diaminobenzidine; brown coloration) or VIP (dark purple coloration) from Vector Laboratories. TUNEL staining was performed according to the manufacturer's (Roche) instructions.

PET scan analyses. PET scan analyses were performed at the Animage imaging department in Lyon (Centre d'Exploration et de Recherche Multimodal et Pluridisciplinaire, France). Animals analyzed by PET imaging belong to an experimental group composed of transplanted animals (4 mo after transplantation) that displayed palpable tumors in the spleen and a high percentage of F4/80-positive HS cells in the peripheral blood. Quantitative PET analyses of four independent animals of each genotype were performed on spleen and liver before (day 0) and after (day 15) *E4F1* inactivation. Clinical grade radiolabeled fluorodeoxyglucose ([^{18}F]FDG) was produced locally using a cyclotron. [^{18}F]FDG uptake was calculated from a whole body acquisition of 30-min length on anesthetized animals performed with a high-resolution small animal PET scanner (Raytest ClearPET; Crystal Clear Collaboration) after i.v. injection of 300 µCi [^{18}F]FDG in 100 µl of 0.9% NaCl solution in tail vein. Acquisition started 2 h after [^{18}F]FDG injection to reduce tracer uptake in the bladder caused by renal excretion. PET scan images were reconstructed and quantified according to the injected amounts of [^{18}F]FDG using the freeware Amide.

Reagents. AO, 3MA, 4OHT, DAPI, propidium iodide (PI), Tiron, collagenase, Hepes, Na pyruvate, Tween 20, and NAC were purchased from Sigma-Aldrich. D3T was purchased from Axxora Platform, and Click-it EdU flow cytometry assay kit, CM-H_2DCFDA, MitoSOX, OxyBURST, and FITC-conjugated avidin were purchased from Invitrogen. Annexin V–FLUOS (herein referred to as annexin V) and BSA were purchased from Roche. RPMI Glutamax-I and FBS were purchased from Invitrogen and Biowest, respectively. For experiments on

HS cell lines and primary macrophages, the working concentrations of the following chemical reagents were used: 1 μg/ml AO, 1 mM 3MA, 3 μM 4OHT, 100 μM Tiron, 200 μM NAC, and 10 μM D3T.

Viability, proliferation, cell death, and ROS detection assays. Viability was determined by manual counting after trypan blue exclusion. The proliferation rate of HS cells was assessed after incubation for 2 h with EdU by FACS analysis with the EdU flow cytometry assay kit (Invitrogen), according to the manufacturer's recommendations. Mitotic cells were identified with the Ser10 phospho–histone H3 antibody (Cell Signaling Technology). Cell death was evaluated by flow cytometry upon annexin V/PI staining. Total and mitochondrial ROS levels were evaluated by flow cytometry or immunofluorescence microscopy, upon staining with CM-H_2DFCDA, OxyBURST, and MitoSOX probes or the MitoSOX probe only, respectively, according to the manufacturer's recommendations. As shown in Fig. 6 A (right), the kinetics of MitoSOX staining were evaluated over a 75-min period. Quantitative data represent the fold increase of time-dependent changes in mean fluorescence intensity of MitoSOX staining measured by flow cytometry. Annexin V/PI and CM-H_2DCFDA/MitoSOX analyses were performed on freshly trypsinized live cells on a flow cytometer (FACSCalibur; BD).

Isolation of HS cell lines and primary macrophages. Four HS cell lines (two *E4F1*$^{+/flox}$ and two *E4F1*$^{-/flox}$) were established ex vivo out of nine lungs and zero out of nine livers harvested from unrecombined *E4F1* KO or CT; *Ink4a/Arf* KO animals, as follows: fresh HSs of appropriate genotype were harvested from transplanted recipient mice of ∼20 wk of age, mechanically dissociated, digested in collagenase for 2 h at 37°C, and then cultured in RPMI Glutamax-I supplemented with 10% IFBS, 2.5 g/l glucose, 10 mM Hepes, and 1 mM Na pyruvate in a humidified 5% CO_2, 37°C incubator. Primary macrophages were harvested by injection of 10 ml PBS in the intraperitoneal cavity of mice of appropriate genotype, centrifuged, and plated for 2 h. Nonadherent cells were removed by repeated washing with culture medium. Purity (>90%) of the adherent macrophage population was evaluated by flow cytometry with Mac2 antibody. Primary macrophages were cultured in the same conditions and medium than HS cells lines. *E4F1* inactivation in HS cell lines and primary macrophages was obtained by the addition of 4OHT to the culture medium, 2 h after plating.

Measurement of oxygen consumption and ATP production. Oxygen consumption was determined by two independent methods. The XF24 Extracellular Flux Analyzer (Seahorse Bioscience), based on fluorimetric sensors, was used for real-time in situ measurement of the OCR in *E4F1* HS cells and primary intraperitoneal macrophages. Analyses were conducted on 80,000 cells/well in triplicate for each cell type (*E4F1* CT or KO HS cells or primary macrophages). Mean values of OCRs were then calculated after correction to the total amount of cellular protein per well. For these experiments, cells were incubated for 1 h at 37°C in HCO_3-free DME containing 25 mM glucose and 1 mM pyruvate. Measurement of OCR was performed over 2 min in three measurement intervals to assess basal metabolic rate, oligomycin C (1 μg/ml final)–sensitive OCR associated to ATP production, and maximal respiratory capacity (upon FCCP [0.3 μM final] followed by rotenone [0.1 μM final] administration). Oxygen consumption was also measured using a temperature-regulated Clark-type O_2 electrode chamber (Strathkelvin Instruments) in murine *E4F1* HS cells and human leukemic cell lines. Oxygen consumption was measured on 5×10^6 cells for 5–15 min (until oxygen consumption ceased) at 37°C in the presence of 2.5 mM malate and 10 mM pyruvate, upon repeated ADP injection (three injections of ADP, 1 mM final). Respiration values were normalized to cell number. For ATP measurements, 20,000 cells were plated in quadruplicates in a 96-well plate, and ATP was measured 3 h later by using the Cell Titer Glo (Promega) luminescent assay. In brief, cells were incubated in the lysis buffer, and the luminescence was determined 10 min later. ATP levels were normalized to total protein levels.

Soft agar assays. Single cell suspensions of HS cells were mixed with RPMI containing 0.4% noble agar and plated on the top of a layer containing 1% noble agar in 6-well plates in triplicate (100,000 cells per plate). Fresh medium, with or without 4OHT, was added every 3 d. Colonies were stained after 3 wk of culture with a 0.5% crystal violet solution and counted.

Immunofluorescence microscopy. In all experiments, HS cells were grown on a glass culture chamber (Falcon; BD). For LC3 immunostaining, cells were fixed with 2% paraformaldehyde for 5–10 min at room temperature, permeabilized by 0.1% Triton X-100 for 5 min at room temperature, incubated for 1 h with a blocking solution of PBS/1.5% BSA, and then stained for 1 h at 37°C with anti-LC3 antibody (Sigma-Aldrich) or overnight at 4°C with anticatalase (Rockland), anti-HO1 (Stressgen), NQO1 (Abcam), and anti-NRF2 (gift from E.E. Schmidt, Montana State University, Bozeman, MT) antibodies. After three washes in PBS/1% BSA/0.1% Tween 20, the slides were incubated for 45 min at 37°C in the dark with FITC-conjugated anti–rabbit secondary antibody. To visualize oxidized DNA (8-OHdG staining), cells were fixed with methanol at −20°C for 20 min and then incubated with 15 μg/ml FITC-conjugated avidin for 1 h at 37°C, as previously described (Radisky et al., 2005). To detect mitochondrial ROS, living cells were first incubated with MitoSOX (5 μM final) for 10 min at 37°C and then fixed with 2% paraformaldehyde. Acidic vesicular organelles were visualized by staining cells with 1 μg/ml AO for 10 min at 37°C. All fixed cells were costained with DAPI for 5 min and mounted in Vectashield imaging medium (Vector Laboratories) before observation with an upright microscope (Axioimager Z1/apotome; Carl Zeiss). MitoSOX images were acquired with a gamma adjustment of 0.55.

Semiquantitative and quantitative immunoblotting. Total protein extracts were prepared by lysing HS cells or intraperitoneal primary macrophages in Triton X-100 lysis buffer (50 mM Tris-HCl, pH 7.4, 100 mM NaCl, 50 mM NaF, 5 mM EDTA, 40 mM β-glycerophosphate, 1 mM Na orthovanadate, 10^{-4} M PMSF, 10^{-6} M leupeptin, 10^{-6} M pepstatin A, and 1% Triton X-100), separated by SDS-PAGE, and transferred to nitrocellulose membranes. Membranes were blocked in TBS containing 5% nonfat milk for 1 h at room temperature and incubated overnight at 4°C with primary antibodies. The following antibodies were used: E4F1 affinity-purified rabbit polyclonal antibody that was generated against the human full-length (aa 1–784) E4F1 protein, antiactin, and anti-LC3 antibodies (Sigma-Aldrich), anti-GAPDH (Santa Cruz Biotechnology, Inc.), anti–phospho-Akt (S473) and anti–total Akt (Cell Signaling Technology), and anti-PTEN (A2B1; Santa Cruz Biotechnology, Inc.). Quantitative analyses with the infrared imaging system (Odyssey; LiCor) was performed using DyLight-conjugated secondary antibodies from Thermo Fisher Scientific. Semiquantitative enhanced chemiluminescence–based immunoblotting was performed using horseradish peroxidase–conjugated secondary antibodies purchased from GE healthcare.

Transmission electron microscopy and ultrastructural evaluation. Adherent HS cells were fixed in 3.5% glutaraldehyde in 0.1 M Sorensen's phosphate buffer, pH 7.4, for 1 h at room temperature. The cells were then scrapped and maintained overnight at 4°C in this fixative solution. After washes in Sorensen's buffer, cells were postfixed in a 1% osmic acid plus 0.8% potassium ferrocyanide for 2 h at room temperature in the dark. After two washes in Sorensen's buffer, the cells were dehydrated in a graded series of ethanol solutions (30–100%) and embedded in EmBed 812 resin. Thin sections (85 nm) were cut on an ultramicrotome (Ultracut E; Leica) and collected at different levels of each block. These sections were counterstained with uranyl acetate and examined on a transmission electron microscope (model 7100; Hitachi).

Lentiviral particles productions and infections. Viral particles were produced in HEK 293T cells by standard procedures after transfection of the following constructs: pLKO1 encoding shRNAs directed against human E4F1 (shE4F1#1, Sigma-Aldrich mission clone 1740s1c1; shE4F1#2, clone 2411s1c1), murine p53 (sh p53, Sigma-Aldrich mission shRNA clone 1526s1c1), or an irrelevant shRNA (sh Ct, clone shc002). 48 h after transfection, viral particles were harvested in the supernatant and added overnight in

the culture medium of *E4F1* HS cells or U937, HEL, HL60, or THP1 human cell lines in the presence of polybrene (8 μg/ml final).

Human samples for E4F1 expression levels evaluation. Anonymous normal and AML BM samples were provided by the Laboratoire d'Hématologie, Hôpital St. Eloi, Centre Hospitalier Universitaire (collection no. DC-2010-1185 approved by the French minister of health). Frozen vials were thawed in complete medium, and whole-cell extracts were prepared in Laemmli buffer containing protease inhibitors. E4F1 and actin protein expression levels were determined by quantitative immunoblotting.

Statistic analyses. Unless otherwise indicated, the unpaired Student's *t* test was used in all analyses, data in bar graphs are represented as mean ± SEM, and statistical significance was expressed as follows: *, $P < 0.05$; **, $P < 0.01$; ***, $P < 0.001$.

Online supplemental material. Fig. S1 describes the HS mouse model used to decipher *E4F1* functions during leukemic development. Fig. S2 illustrates tumor regression occurring upon *E4F1* inactivation. Fig. S3 shows deregulation of the PI3K pathway in HS cell lines. Fig. S4 shows the immunophenotypic characterization of HS cell lines. Fig. S5 shows the impact of caspase inhibitor and antioxidant molecules on cell death of *E4F1* KO HS cells. Fig. S6 shows the induction of a cellular antioxidant response upon *E4F1* inactivation in HS cells. Fig. S7 shows the role of p53 in cell death occurring in *E4F1* KO HS cells. Fig. S8 shows the overexpression of E4F1 in murine HS cell lines and human AML samples. Online supplemental material is available at http://www.jem.org/cgi/content/full/jem.20101995/DC1.

We thank the Réseau d'Histologie Expérimentale de Montpellier histology facility and Patricia Cavelier for processing our animal tissues, Animage in vivo imaging core facility (Lyon, France) for PET scan analyses, Montpellier Rio Imaging for cell imaging, and the Centre Régional d'Imagerie Cellulaire facilities for ultrastructure microscopy (Montpellier, France). We also thank Eric Jouffre, Marc Plays, and Karim Chebli for technical help in mouse handling, M. Barbacid and M. Serrano for providing us with the *Ink4a/Arf* KO and *RERT* KI strains of mice, S. Pattingre and Lucille Espert for valuable discussions on autophagy, and S. Thevenin for statistical analyses. We are grateful to all members of the L. Le Cam, C. Sardet, and L. Fajas laboratories for helpful discussions and critical readings of the manuscript.

This work was supported by the Agence Nationale pour la Recherche, the Association pour la lutte contre le Cancer (ARC), the Leukemia Program from the Fondation de France, the British Association for International Cancer Research (AICR) foundation, and la Fondation pour la Recherche Médicale (C. Sardet équipe labelisée 2007) and the institutional supports of the Institut National de la Santé et de la Recherche Médicale Avenir Program (L. Le Cam) and the Centre National de la Recherche Scientifique (C. Sardet). E. Hatchi and J. Caramel are supported by an ARC PhD and AICR postdoctoral fellowship, respectively.

The authors have no conflicting financial interests.

Submitted: 22 September 2010
Accepted: 18 May 2011

REFERENCES

Ahmed-Choudhury, J., A. Agathanggelou, S.L. Fenton, C. Ricketts, G.J. Clark, E.R. Maher, and F. Latif. 2005. Transcriptional regulation of cyclin A2 by RASSF1A through the enhanced binding of p120E4F to the cyclin A2 promoter. *Cancer Res.* 65:2690–2697. doi:10.1158/0008-5472.CAN-04-3593

Berger, J.H., and N. Bardeesy. 2007. Modeling INK4/ARF tumor suppression in the mouse. *Curr. Mol. Med.* 7:63–75. doi:10.2174/156652407779940477

Carrasco, D.R., T. Fenton, K. Sukhdeo, M. Protopopova, M. Enos, M.J. You, D. Di Vizio, C. Nogueira, J. Stommel, G.S. Pinkus, et al. 2006. The PTEN and INK4A/ARF tumor suppressors maintain myelolymphoid homeostasis and cooperate to constrain histiocytic sarcoma development in humans. *Cancer Cell.* 9:379–390. doi:10.1016/j.ccr.2006.03.028

Chagraoui, J., S.L. Niessen, J. Lessard, S. Girard, P. Coulombe, M. Sauvageau, S. Meloche, and G. Sauvageau. 2006. E4F1: a novel candidate factor for mediating BMI1 function in primitive hematopoietic cells. *Genes Dev.* 20:2110–2120. doi:10.1101/gad.1453406

Colombo, R., G.F. Draetta, and S. Chiocca. 2003. Modulation of p120E4F transcriptional activity by the Gam1 adenoviral early protein. *Oncogene.* 22:2541–2547. doi:10.1038/sj.onc.1206379

Crighton, D., S. Wilkinson, J. O'Prey, N. Syed, P. Smith, P.R. Harrison, M. Gasco, O. Garrone, T. Crook, and K.M. Ryan. 2006. DRAM, a p53-induced modulator of autophagy, is critical for apoptosis. *Cell.* 126:121–134. doi:10.1016/j.cell.2006.05.034

Dudziak, K., N. Mottalebi, S. Senkel, E.L. Edghill, S. Rosengarten, M. Roose, C. Bingham, S. Ellard, and G.U. Ryffel. 2008. Transcription factor HNF1beta and novel partners affect nephrogenesis. *Kidney Int.* 74:210–217. doi:10.1038/ki.2008.149

Eischen, C.M., J.E. Rehg, S.J. Korsmeyer, and J.L. Cleveland. 2002. Loss of Bax alters tumor spectrum and tumor numbers in ARF-deficient mice. *Cancer Res.* 62:2184–2191.

Fajas, L., C. Paul, O. Zugasti, L. Le Cam, J. Polanowska, E. Fabbrizio, R. Medema, M.L. Vignais, and C. Sardet. 2000. pRB binds to and modulates the trans-repressing activity of the E1A-regulated transcription factor p120E4F. *Proc. Natl. Acad. Sci. USA.* 97:7738–7743. doi:10.1073/pnas.130198397

Fajas, L., C. Paul, A. Vié, S. Estrach, R. Medema, J.M. Blanchard, C. Sardet, and M.L. Vignais. 2001. Cyclin A is a mediator of p120E4F-dependent cell cycle arrest in G1. *Mol. Cell. Biol.* 21:2956–2966. doi:10.1128/MCB.21.8.2956-2966.2001

Fenton, S.L., A. Dallol, A. Agathanggelou, L. Hesson, J. Ahmed-Choudhury, S. Baksh, C. Sardet, R. Dammann, J.D. Minna, J. Downward, et al. 2004. Identification of the E1A-regulated transcription factor p120 E4F as an interacting partner of the RASSF1A candidate tumor suppressor gene. *Cancer Res.* 64:102–107. doi:10.1158/0008-5472.CAN-03-2622

Fernandes, E.R., J.Y. Zhang, and R.J. Rooney. 1998. Adenovirus E1A-regulated transcription factor p120E4F inhibits cell growth and induces the stabilization of the cdk inhibitor p21WAF1. *Mol. Cell. Biol.* 18:459–467.

Guerra, C., N. Mijimolle, A. Dhawahir, P. Dubus, M. Barradas, M. Serrano, V. Campuzano, and M. Barbacid. 2003. Tumor induction by an endogenous K-ras oncogene is highly dependent on cellular context. *Cancer Cell.* 4:111–120. doi:10.1016/S1535-6108(03)00191-0

Huang, P., L. Feng, E.A. Oldham, M.J. Keating, and W. Plunkett. 2000. Superoxide dismutase as a target for the selective killing of cancer cells. *Nature.* 407:390–395. doi:10.1038/35030140

Huang, Q., Y.T. Wu, H.L. Tan, C.N. Ong, and H.M. Shen. 2009. A novel function of poly(ADP-ribose) polymerase-1 in modulation of autophagy and necrosis under oxidative stress. *Cell Death Differ.* 16:264–277. doi:10.1038/cdd.2008.151

Kamijo, T., F. Zindy, M.F. Roussel, D.E. Quelle, J.R. Downing, R.A. Ashmun, G. Grosveld, and C.J. Sherr. 1997. Tumor suppression at the mouse INK4a locus mediated by the alternative reading frame product p19ARF. *Cell.* 91:649–659. doi:10.1016/S0092-8674(00)80452-3

Khoo, C.M., D.R. Carrasco, M.W. Bosenberg, J.H. Paik, and R.A. Depinho. 2007. Ink4a/Arf tumor suppressor does not modulate the degenerative conditions or tumor spectrum of the telomerase-deficient mouse. *Proc. Natl. Acad. Sci. USA.* 104:3931–3936. doi:10.1073/pnas.0700093104

Kim, W.Y., and N.E. Sharpless. 2006. The regulation of INK4/ARF in cancer and aging. *Cell.* 127:265–275. doi:10.1016/j.cell.2006.10.003

Klaunig, J.E., L.M. Kamendulis, and B.A. Hocevar. 2010. Oxidative stress and oxidative damage in carcinogenesis. *Toxicol. Pathol.* 38:96–109. doi:10.1177/0192623309356453

Koopman, W.J., L.G. Nijtmans, C.E. Dieteren, P. Roestenberg, F. Valsecchi, J.A. Smeitink, and P.H. Willems. 2010. Mammalian mitochondrial complex I: biogenesis, regulation, and reactive oxygen species generation. *Antioxid. Redox Signal.* 12:1431–1470. doi:10.1089/ars.2009.2743

Lacroix, M., J. Caramel, P. Goguet-Rubio, L.K. Linares, S. Estrach, E. Hatchi, G. Rodier, G. Lledo, C. de Bettignies, A. Thépot, et al. 2010. Transcription factor E4F1 is essential for epidermal stem cell maintenance and skin homeostasis. *Proc. Natl. Acad. Sci. USA.* 107:21076–21081. doi:10.1073/pnas.1010167107

Le Cam, L., M. Lacroix, M.A. Ciemerych, C. Sardet, and P. Sicinski. 2004. The E4F protein is required for mitotic progression during embryonic cell cycles. *Mol. Cell. Biol.* 24:6467–6475. doi:10.1128/MCB.24.14.6467-6475.2004

Le Cam, L., L.K. Linares, C. Paul, E. Julien, M. Lacroix, E. Hatchi, R. Triboulet, G. Bossis, A. Shmueli, M.S. Rodriguez, et al. 2006. E4F1 is an atypical ubiquitin ligase that modulates p53 effector functions independently of degradation. *Cell*. 127:775–788. doi:10.1016/j.cell.2006.09.031

Lee, K.A., and M.R. Green. 1987. A cellular transcription factor E4F1 interacts with an E1a-inducible enhancer and mediates constitutive enhancer function in vitro. *EMBO J.* 6:1345–1353.

Lee, K.A., T.Y. Hai, L. SivaRaman, B. Thimmappaya, H.C. Hurst, N.C. Jones, and M.R. Green. 1987. A cellular protein, activating transcription factor, activates transcription of multiple E1A-inducible adenovirus early promoters. *Proc. Natl. Acad. Sci. USA*. 84:8355–8359. doi:10.1073/pnas.84.23.8355

Levine, B., and G. Kroemer. 2008. Autophagy in the pathogenesis of disease. *Cell*. 132:27–42. doi:10.1016/j.cell.2007.12.018

Lund, A.H., G. Turner, A. Trubetskoy, E. Verhoeven, E. Wientjens, D. Hulsman, R. Russell, R.A. DePinho, J. Lenz, and M. van Lohuizen. 2002. Genome-wide retroviral insertional tagging of genes involved in cancer in Cdkn2a-deficient mice. *Nat. Genet.* 32:160–165. doi:10.1038/ng956

Martín-Caballero, J., J.M. Flores, P. García-Palencia, and M. Serrano. 2001. Tumor susceptibility of p21(Waf1/Cip1)-deficient mice. *Cancer Res.* 61:6234–6238.

Mizushima, N. 2009. Physiological functions of autophagy. *Curr. Top. Microbiol. Immunol.* 335:71–84. doi:10.1007/978-3-642-00302-8_3

Nogueira, V., Y. Park, C.C. Chen, P.Z. Xu, M.L. Chen, I. Tonic, T. Unterman, and N. Hay. 2008. Akt determines replicative senescence and oxidative or oncogenic premature senescence and sensitizes cells to oxidative apoptosis. *Cancer Cell*. 14:458–470. doi:10.1016/j.ccr.2008.11.003

Nojima, J., K. Kanomata, Y. Takada, T. Fukuda, S. Kokabu, S. Ohte, T. Takada, T. Tsukui, T.S. Yamamoto, H. Sasanuma, et al. 2010. Dual roles of smad proteins in the conversion from myoblasts to osteoblastic cells by bone morphogenetic proteins. *J. Biol. Chem.* 285:15577–15586. doi:10.1074/jbc.M109.028019

Paul, C., M. Lacroix, I. Iankova, E. Julien, B.W. Schäfer, C. Labalette, Y. Wei, A. Le Cam, L. Le Cam, and C. Sardet. 2006. The LIM-only protein FHL2 is a negative regulator of E4F1. *Oncogene*. 25:5475–5484. doi:10.1038/sj.onc.1209567

Quelle, D.E., F. Zindy, R.A. Ashmun, and C.J. Sherr. 1995. Alternative reading frames of the INK4a tumor suppressor gene encode two unrelated proteins capable of inducing cell cycle arrest. *Cell*. 83:993–1000. doi:10.1016/0092-8674(95)90214-7

Radisky, D.C., D.D. Levy, L.E. Littlepage, H. Liu, C.M. Nelson, J.E. Fata, D. Leake, E.L. Godden, D.G. Albertson, M.A. Nieto, et al. 2005. Rac1b and reactive oxygen species mediate MMP-3-induced EMT and genomic instability. *Nature*. 436:123–127. doi:10.1038/nature03688

Raychaudhuri, P., R. Rooney, and J.R. Nevins. 1987. Identification of an E1A-inducible cellular factor that interacts with regulatory sequences within the adenovirus E4 promoter. *EMBO J.* 6:4073–4081.

Rizos, H., E. Diefenbach, P. Badhwar, S. Woodruff, T.M. Becker, R.J. Rooney, and R.F. Kefford. 2003. Association of p14ARF with the p120E4F transcriptional repressor enhances cell cycle inhibition. *J. Biol. Chem.* 278:4981–4989. doi:10.1074/jbc.M210978200

Rooney, R.J. 2001. Cell cycle attenuation by p120E4F is accompanied by increased mitotic dysfunction. *Cell Growth Differ.* 12:505–516.

Rui, E., P.R. Moura, K.A. Gonçalves, R.J. Rooney, and J. Kobarg. 2006. Interaction of the hepatitis B virus protein HBx with the human transcription regulatory protein p120E4F in vitro. *Virus Res.* 115:31–42. doi:10.1016/j.virusres.2005.07.003

Sandy, P., M. Gostissa, V. Fogal, L.D. Cecco, K. Szalay, R.J. Rooney, C. Schneider, and G. Del Sal. 2000. p53 is involved in the p120E4F-mediated growth arrest. *Oncogene*. 19:188–199. doi:10.1038/sj.onc.1203250

Serrano, M., H. Lee, L. Chin, C. Cordon-Cardo, D. Beach, and R.A. DePinho. 1996. Role of the INK4a locus in tumor suppression and cell mortality. *Cell*. 85:27–37. doi:10.1016/S0092-8674(00)81079-X

Sharpless, N.E., N. Bardeesy, K.H. Lee, D. Carrasco, D.H. Castrillon, A.J. Aguirre, E.A. Wu, J.W. Horner, and R.A. DePinho. 2001. Loss of p16Ink4a with retention of p19Arf predisposes mice to tumorigenesis. *Nature*. 413:86–91. doi:10.1038/35092592

Struthers, L., R. Patel, J. Clark, and S. Thomas. 1998. Direct detection of 8-oxodeoxyguanosine and 8-oxoguanine by avidin and its analogues. *Anal. Biochem.* 255:20–31. doi:10.1006/abio.1997.2354

Sundström, C., and K. Nilsson. 1976. Establishment and characterization of a human histiocytic lymphoma cell line (U-937). *Int. J. Cancer*. 17:565–577. doi:10.1002/ijc.2910170504

Tasdemir, E., M.C. Maiuri, L. Galluzzi, I. Vitale, M. Djavaheri-Mergny, M. D'Amelio, A. Criollo, E. Morselli, C. Zhu, F. Harper, et al. 2008. Regulation of autophagy by cytoplasmic p53. *Nat. Cell Biol.* 10:676–687. doi:10.1038/ncb1730

Tessari, M.A., M. Gostissa, S. Altamura, R. Sgarra, A. Rustighi, C. Salvagno, G. Caretti, C. Imbriano, R. Mantovani, G. Del Sal, et al. 2003. Transcriptional activation of the cyclin A gene by the architectural transcription factor HMGA2. *Mol. Cell. Biol.* 23:9104–9116. doi:10.1128/MCB.23.24.9104-9116.2003

Trachootham, D., Y. Zhou, H. Zhang, Y. Demizu, Z. Chen, H. Pelicano, P.J. Chiao, G. Achanta, R.B. Arlinghaus, J. Liu, and P. Huang. 2006. Selective killing of oncogenically transformed cells through a ROS-mediated mechanism by beta-phenylethyl isothiocyanate. *Cancer Cell*. 10:241–252. doi:10.1016/j.ccr.2006.08.009

Trachootham, D., H. Zhang, W. Zhang, L. Feng, M. Du, Y. Zhou, Z. Chen, H. Pelicano, W. Plunkett, W.G. Wierda, et al. 2008. Effective elimination of fludarabine-resistant CLL cells by PEITC through a redox-mediated mechanism. *Blood*. 112:1912–1922. doi:10.1182/blood-2008-04-149815

Valko, M., D. Leibfritz, J. Moncol, M.T. Cronin, M. Mazur, and J. Telser. 2007. Free radicals and antioxidants in normal physiological functions and human disease. *Int. J. Biochem. Cell Biol.* 39:44–84. doi:10.1016/j.biocel.2006.07.001

Vousden, K.H., and K.M. Ryan. 2009. p53 and metabolism. *Nat. Rev. Cancer*. 9:691–700. doi:10.1038/nrc2715

Xu, Y., S.O. Kim, Y. Li, and J. Han. 2006. Autophagy contributes to caspase-independent macrophage cell death. *J. Biol. Chem.* 281:19179–19187. doi:10.1074/jbc.M513377200

Zhu, H., L. Zhang, K. Itoh, M. Yamamoto, D. Ross, M.A. Trush, J.L. Zweier, and Y. Li. 2006. Nrf2 controls bone marrow stromal cell susceptibility to oxidative and electrophilic stress. *Free Radic. Biol. Med.* 41:132–143. doi:10.1016/j.freeradbiomed.2006.03.020

Ziech, D., R. Franco, A. Pappa, and M.I. Panayiotidis. 2011. Reactive Oxygen Species (ROS)—Induced genetic and epigenetic alterations in human carcinogenesis. *Mutat. Res.* 711:167–173.